EFFECT OF STRESS RATIO ON FATIGUE CRACK GROWTH RATE AT NOTCHED HOLE IN 7075-T6 ALUMINUM ALLOY UNDER BIAXIAL FATIGUE

THESIS

Alshahrani, Reja

Captain, Royal Saudi Air Force, RSAF

August 2016

DEPARTMENT OF THE AIR FORCE

AIR UNIVERSITY

AIR FORCE INSTITUTE OF TECHNOLOGY

Wright-Patterson Air Force Base, Ohio

DISTRIBUTION STATEMENT A

APPROVED FOR PUBLIC RELEASE; DISTRIBUTION IS UNLIMITED

AFIT-ENY-MS-16-S-052

EFFECT OF STRESS RATIO ON FATIGUE CRACK GROWTH RATE AT NOTCHED HOLE IN 7075-T6 ALUMINUM ALLOY UNDER BIAXIAL FATIGUE

THESIS

Presented to the Faculty

Department of Aeronautics and Astronautics

Graduate School of Engineering and Management

Air Force Institute of Technology

Air University

Air Education and Training Command

In Partial Fulfillment of the Requirements for the

Degree of Master of Science in Materials Science

Alshahrani, Reja
Captain, Royal Saudi Air Force, RSAF

Aug 2016

AFIT-ENY-MS-16-S-052

To my father who passed away in 2015, I missed his prayers for me since then. Thank you for being a great father and to my mother for her encouragement and love- Thank you all.

Abstract

This research investigates the behavior of fatigue crack growth rate in both laboratory air and saltwater (3.5% NaCl) environments for pre-cracked notched cruciform specimen made from 7075-T6 aluminum alloy sheet at different stress ratios. With biaxility ratio of 1, and frequency of applied load of 10 Hz, the crack growth behavior was investigated under in-plane biaxial tension-tension fatigue with 0.1, 0.5, 0.7 stress ratios and then compared them to study the effect of stress ratio on the crack growth rate. Finite Element Analysis (FEA) was used to calculate cyclic variation of stress intensity factors (ΔK) at the crack tips. The crack growth rate was observed using optical microscopy. In addition, the test generates more accurate definition of the Walker equation parameters and leads to more accurate prediction of fatigue crack growth rate at different stress ratio. This study shows that there is no effect of the stress ratio on crack path direction. Increase in stress ratio leads to increase in the fatigue crack growth rate under the biaxial loading test. The effective fatigue crack growth rate predicted by Walker equation is very close to the effective fatigue crack growth rate generated by the test in laboratory air and saltwater environments. In the saltwater environment, the corrosion accelerates the crack growth rate.

Acknowledgments

I would like to express the deepest appreciation to my advisor, Dr. Shankar Mall, for his support and guidance throughout my thesis. Without his knowledge, useful comments, and encouragement this thesis would not have been possible.

I would like to extend my gratitude to Dr. Volodymyr Sabelkin who reviewed my thesis as a reader. Also, I would like to thank Dr. Victor Perel and Capt. Ali Khawagi, who introduced me to the finite element program Abaqus and showed me the proper way of preparing the specimens and executing corrosion fatigue experiments.

In addition, I would like to thank my mother, brothers, and sisters for their love and encouragement. I would like to thank my wife and my sons for their love, support, patience, and for understanding the long hours I spent studying.

Alshahrani, Reja

Table of Contents

List of Figures

Figure Page

List of Tables

Table Page

List of Symbols

Symbol	Definition
a	crack length (mm)
α	angle between the y-axis and the crack (degree)
φ	angle between the x-axis and the crack ($\varphi = 90 - \alpha$) (degree)
b	width of specimen (mm)
C	constant for Paris law (unit less)
CF	corrosion fatigue
Δ	change in a variable (unit less)
da/dN	rate of crack growth per cycle (m/cycle)
DOD	Department of Defense
E	modulus of elastisity
EDM	electric-discharge method
ê	unit basis vectors of the original coordinate system
ê′	unit basis vectors of the rotated coordinate system
F_x	applied force in the x-direction (N)
F_y	applied force in the y-direction (N)
I	mode one (opening)
K	stress intensity factor (MPa*m^0.5)
N	number of cycles
q	mapping the components of a vector onto the components of the same vector in a second coordinate system

R	stress ratio for cyclic loading (unit less)
r	radius of the circular hole (m)
$S_{xx}=S_x$	remote normal stresses at a long distance from the crack tip in the x-direction with respect to the global coordinate system (xy plane) (N/m^2)
$S_{yy}=S_y$	remote normal stresses at a long distance from the crack tip in the y-direction with respect to the global coordinate system (xy plane) (N/m^2)
S_{xy}	remote shear stresses at a long distance from the crack tip with respect to the global coordinate system (xy plane) (N/m^2)
S'_{xx}	remote normal stresses at a long distance from the crack tip in the x-direction with respect to the local rectangular coordinate system ($x'y'$ plane) (N/m^2)
S'_{yy}	remote normal stresses at a long distance from the crack tip in the y-direction with respect to the local rectangular coordinate system ($x'y'$ plane) (N/m^2)
S'_{xy}	remote shear stresses at a long distance from the crack tip with respect to the local rectangular coordinate system ($x'y'$ plane) (N/m^2)
$S_{\rho\rho}$	remote normal stresses at a long distance from the crack tip at angle of θ with respect to the local polar coordinate system ($\rho\theta$ plane) (N/m^2)
$S_{\theta\theta}$	remote normal stresses at a long distance from the crack tip at an angle of $\theta + 90°$ with respect to the local polar coordinate system ($\rho\theta$ plane) (N/m^2)
$S_{\rho\theta}$	remote shear stresses at a long distance from the crack tip with respect to the local polar coordinate system ($\rho\theta$ plane) (N/m^2)

σ	stress (MPa)
σ'_{xx}	normal stresses near the crack tip in the x-direction with respect to the local rectangular coordinate system (x′y′ plane) (N/m^2)
σ'_{yy}	normal stresses near the crack tip in the y-direction with respect to the local rectangular coordinate system (x′y′ plane) (N/m^2)
σ'_{xy}	shear stresses near the crack tip in with respect to the local rectangular coordinate system (x′y′ plane) (N/m^2)
$\sigma_{\rho\rho}$	normal stresses near the crack tip at an angle of θ from the local rectangular coordinate system (x′y′ plane) and with respect to the local polar coordinate system (ρθ plane) (N/m^2)
$\sigma_{\theta\theta}$	normal stresses near the crack tip at an angle of $\theta + 90°$ from the local rectangular coordinate system (x′y′ plane) and with respect to the local polar coordinate system (ρθ plane) (N/m^2)
$\sigma_{\rho\theta}$	shear stresses near the crack tip with respect to the local polar coordinate system (ρθ plane) (N/m^2)
T	stress tensor
T′	transformed stress tensor
t	thickness of specimen (mm)
w	width of specimen (mm)
ω	frequency of the applied load
ν	Poisson's ratio
λ	global biaxiality ratio

λ' local biaxiality ratio

EFFECT OF STRESS RATIO ON FATIGUE CRACK GROWTH RATE AT NOTCHED HOLE IN 7075-T6 ALUMINUM ALLOY UNDER BIAXIAL FATIGUE

I. Introduction

1.1 Corrosion

Corrosion is considered to be the most common concerns when it comes to raise efficiency of metals products or reduce their cost of operation, it can create huge damage to the metals. As the Number of commercial airplanes, fighter aircrafts and unmanned aerial vehicles increase with time, the cost of corrosion and life of these aircraft become big issue.

Approximately, United States spend $276 Billion [11, 14] and it is 3.1% of its Gross National product each year to the corrosion. Corrosion cost is challenging, even when its effects on readiness and safety are excluded [14]. Figure 1 indicates the cost of corrosion in the most of organizations that suffer from corrosion.

The United States Department of Defense (DoD) it deals directly with corrosion and it spends more than $22.5 Billion each year fighting the corrosion by using the materials, man hours, training and preparing corrosion facilities to make researches to control and prevent corrosion [14].

Due to the huge amount of aircraft fleet in The United State Air Force it has the big share suffering from corrosion, the cost of corrosion reached in 2009 $ 5.4 Billion and affect the readiness of the Air Force and shorten the aircrafts life cycle as well as the safety issues [14].

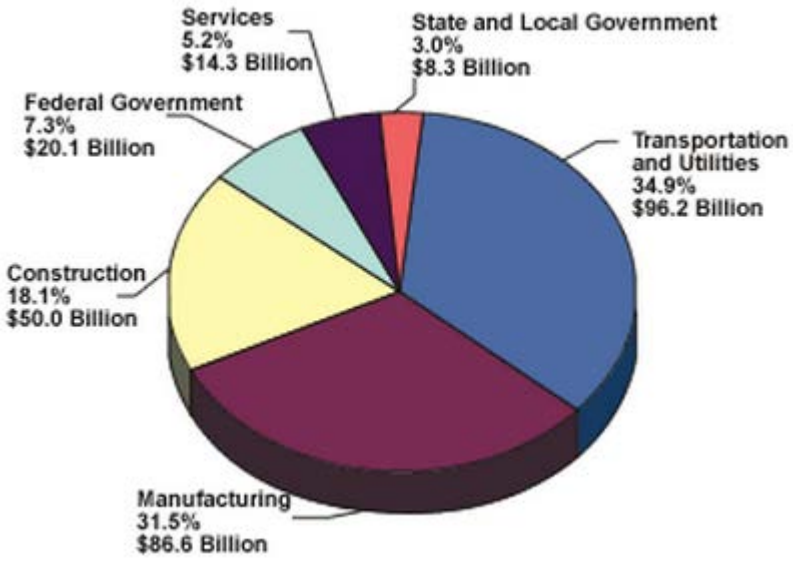

Figure 1: Cost of corrosion in different categories of industry [2].

Corrosion is a process in which metallic material is deteriorate due to reaction between the metal and its environment which results in changes in the consumption of a material, or it can be a chemical reaction cause the material to loss it's physical properties and it weakening the material due to a loss in cross-section or reduce the thickness leads to loss in mechanical strength and fail in structure [31]. Metals corrode because they are chemically unstable in the environments where they have been used. To control or prevent corrosion there must be an understanding of the kind of corrosion, and there are many methods of controlling corrosion such as painting, coatings, chemical inhibitors, materials selection, cathodic method and even washing the metals by clear water helps to control corrosion [31, 35]. Figure 2 shows washing an F15 to remove the dust which control corrosion.

Figure 2: Washing an F-15 to remove dust to control corrosion.

One of the most common metals that resist corrosion is aluminum alloy and it has been used to build aircrafts structure due to many factors such as its light weight, low cost, resistance to corrosion unless it is exposed to acidic solutions and it is flexible to take any shape. And this is the reason to be the scope of this study. [25]

1.2 Corrosion Fatigue

Fatigue can be defined as the process of damage and failure due to cyclic loading, and this cyclic loading is result of repeated loads. Even at stresses below ultimate strength of materials cyclic loading develops a crack which leads to failure [33]. As mentioned before, the corrosion weakens the materials and also accelerates the crack growth rate. From that combined factors of failures as corrosion and cyclic loading failure occurs much sooner. Also the failure occurs under lower number of cycles leads to shorten life cycle time and that is corrosion fatigue [2].

1.3 Biaxial Corrosion Fatigue

Since the scientists started studying crack in all of its modes, initiation, propagation, failure, and the effect of environment in crack growth most of them used uniaxial loading. And that give good understanding of crack behavior [26]. But when aircrafts industries face the fact of losing a lot of money replacing damaged parts due to corrosion fatigue before its lifetime they have many questions that have to be answered. One of them is why the structure fails before its time, how can they extend the lifetime of the structure or at least how can I prevent of delay failure.

In fact, when aircraft fly or perform any kind of maneuvering the structures exposed to different types of loads and moments in different directions. And that not in an ideal environment, corrosive environment while enhance and accelerate the crack initiation and propagation and that will result corrosion fatigue failure in a time less than what the structure supposed to be fail. And that give the importance of studying structure in cyclic loading and understand the effect of corrosion in crack under biaxial loading.

The damage tolerance approach has been used to study the propagation of cracks and follows the assumption that weakness is present in all structures due to cyclic loading and corrosion. This approach has been used to delay crack in structure in aerospace field [26].

In addition, laterally many studies have described the influence of biaxial loading on fatigue crack growth rate [18,27]. One of common loading conditions that aircraft experience is in-plane stress. Taylor and Lee studied the effect of in-plane stress biaxility on the fatigue life [22]. Research in this subject is going on but no research done to study

the effect of different stresses ratio in air and corrosive environment and released to public until now. Several studies of an in-plane biaxial fatigue crack growth of aluminum alloy had been conducted to give a better understanding of crack growth rate generated from rivet holes or bolted joints in saltwater environment by Dr. Mall and his team [27].

1.4 Problem Statement

The crack growth behavior can be described by the relationship between cyclic crack growth rate *da/dN* and stress intensity range *ΔK* for a given material and set of test conditions [33]. The relationship in expressed in Paul Paris equation

$$\frac{da}{dN} = C(\Delta k)^m \qquad (1.1)$$

where C is constant and *m* is the slop on the log-log plot [33]. Crack growth test are commonly conducted under zero-to-tension loading, *R*=0, or tension-to-tension loading with a small value of *R.* the data are obtained from uniaxial stress tests in air [33]. Barsom (1999) studied various classes of steel for variation of *R* from 0 to 0.2 under uniaxial cyclic load. But aircraft structures face several types of stress during the flight, researches started collecting data of crack growth under an in-plane biaxial fatigue condition in air and corrosive environment [12,26,27]. In those tests data gained and analyzed with different biaxility ratios in air and saltwater environment and 0.5 stress ratio,10 Hz frequency [26,27]. None of these tests studied the effect of changing tension-to-tension load (stress ratio *R*) in fatigue crack growth and described the relationship between cyclic crack growth rate *da/dN* and stress intensity range *ΔK* which is the scope of this research, using fracture mechanics approach.

To achieve the purpose of this study, the specimen has to be test under in-plane biaxial loading with same experimental setup and changing R-ratio every time to study the effect of that in fatigue crack growth.

7075-T6 aluminum alloy was selected to be the material used in this test because it is the most common material used in aircraft structure [27]. Fatigue crack growth behavior was examined under in-plane biaxial loading in saltwater (3.5% NaCl) and air environment.

The specimen is machined from 7075-T6 aluminum alloy sheet, with 6 mm diameter hole in center, a 45° to horizontal notch was originating from the hole with 1 mm length and 0.25 mm width. The specimen arm length is 120 mm and width was 45 mm to fit in the Fatigue testing machine.

The test starts with precracking the specimen 1 mm form the notch for all used specimens to obtain the accuracy in reading data and to check if there are any defects in the specimen with biaxiality ratio of 1 ($\lambda = 1$) to control the data range, the stresses were calculated for each R-ratio to obtain same starting point for all experiments. Then, the crack growth rate has been measured with the number of cycles to failure for each experiment for R-ratios (R= 0.1, 0.5, 0.7). In order to study the behavior of the cracks, the finite element analysis was used to calculate the range of stress intensity factor (ΔK).

This study presented valuable information about fatigue crack growth behavior for wide range of stress ratio in air and corrosive environment to compare different

loading conditions. And it is a link between previous studies and future studies in the field.

II. Background

2.1 Fatigue

Since fracture mechanics begin, improving the structure by increasing the strength was the core of the study in parallel with extending the lifetime of the structure. But pushing the structure to its' limit cause another major issue incidentally occurs which called fatigue. Fracture mechanics scientists' defined fatigue as the process of damage and failure due to cyclic loading, and this cyclic loading is result of repeated loads. Even at stresses below ultimate strength of materials cyclic loading develops a crack which leads to failure [33]. In fact, there is no aircraft structure free from cracks and these cracks grow with time and that phenomena called structural fatigue.

According to Griffith theory, failure occur before expected time if crack become large enough to propagate in unsteady behavior and it is disaster [36]. Under cyclic load below the material strength point crack growth is steady, but other forms of stresses such as rotation, torsion, pending can lead to fatigue failure [5,34].

Fatigue crack start as invisible microcrack at the weak point of the surface of the structure and that location called the concentrated stresses point, due to those stresses intrusions and extrusion will occur generating small cyclic step along slip planes and that will cause after certain number of cycles shear stress 45^0 angle with the load direction, and that is the end of the first stage called crack initiation. Macrocrack takes

place and connects those small steps together due to high shear stress and crack no longer at surface it takes place inside the structure and the crack propagate with 90^0 angle to the load direction and that called crack propagation stage.

In this stage the crack grows and that leads to third stage where the fracture toughness is exceeded and the fracture fails due to fatigue failure [32]. Figure 3 shows first and second stages of fatigue crack [50].

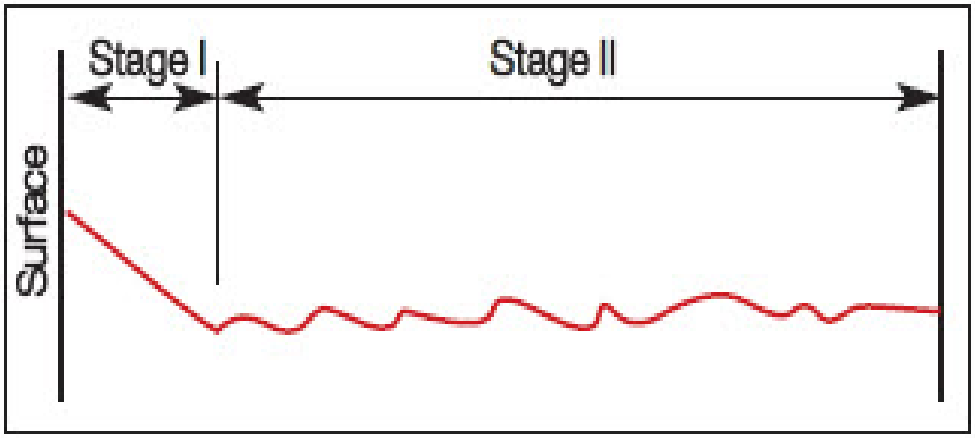

Figure 3: : First and second stages of fatigue crack [50].

2.2 Corrosion Fatigue

Fatigue as described in the previous topic, the weakness of the structure due to cyclic loads for period of a time, and that time depends upon many scales and factors, and this is the importance of studying the behavior of metals. One of the major factors that lead structure to fail before its' lifetime is corrosion. Corrosion accelerates crack growth rate. So, whenever there is fatigue in corrosive environment the failure will occur sooner

than air environment. In fact, corrosion fatigue can be defined as the damage or failure of structure in corrosive environment.

7075-T6 aluminum alloy is designed to work in corrosive environment due to the coating methods. Those protective coating works as a barrier layers to avoid the occurrence of the cathode reaction on the surface. In fact, corrosion effects start when there is direct contact between the cracked area with the corrosive environment. For example, notch or flaw is exposed to corrosive environment and the material defiantly corrode due to creation of hydrogen ions and that reduces the structure binding forces. Defiantly, in present of a crack in this situation hydrogen ions pass through the structure lattice resulting embrittlement. And embrittlement in general is losing the ductility and that means corrosion eliminates the alloy properties and lower fatigue stress and accelerate crack initiation and propagation. This mechanism is called hydrogen embrittlement [13]. Figure 4 shows how hydrogen ions gather forming the embrittlement [5].

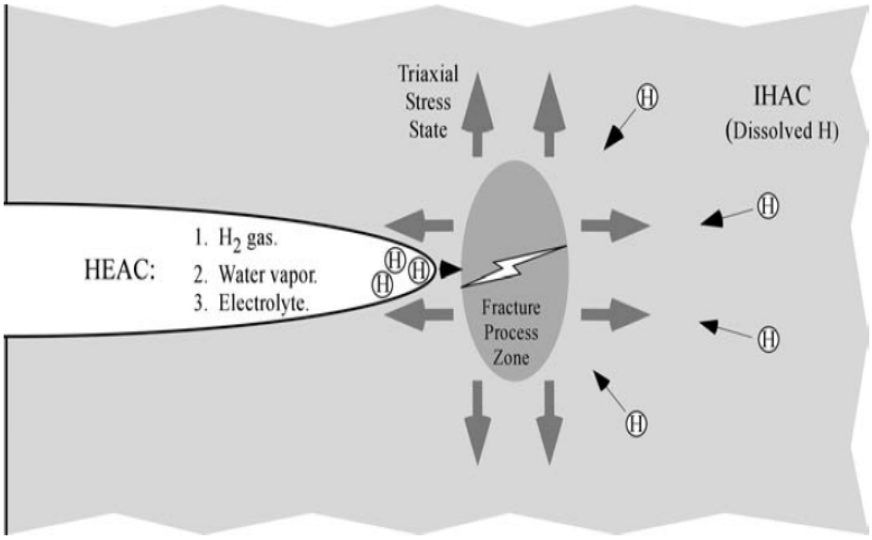

Figure 4: Hydrogen embrittlement mechanism [5].

In fact, knowing the type of loading is very important to differentiate between corrosion fatigue and stress corrosion cracking. Load is oscillated in corrosion fatigue and is stable in stress corrosion crack [47].

2.3 Effect of Corrosion on Fatigue Life

Synergetic damage is that damage where cyclic loading combined with corrosive environment and that cause damage more summing those damages separately [45]. In fact, fatigue life of the material is short in corrosive environment and that because corroded area considered to be the weakest area and that help initiating cracks faster than air environment. In presence of crack, the corrosion passes through the material and the area near the crack corrode until it become oxidized and inactive of corrosion, crack grows distract this area and allow corrosive environment to start corroding new area and

that phenomena repeats itself causing an increase in the crack growth rate and this leads to failure in the structure in very short time [45].

In case of comparing the effect of fatigue in different environments, tow common concept should be considered. First one, the maximum value of stress that material can sustain with no failure and that known as fatigue limit. The second one, the structure' number of cycles to failure and that know as fatigue life. And from experiments with different loads and conditions, these values are reduced in corrosive environment and that result fast failure of structure in corrosive environment. Figure 5 shows the effect of environment in fatigue limit and fatigue life of same material [45].

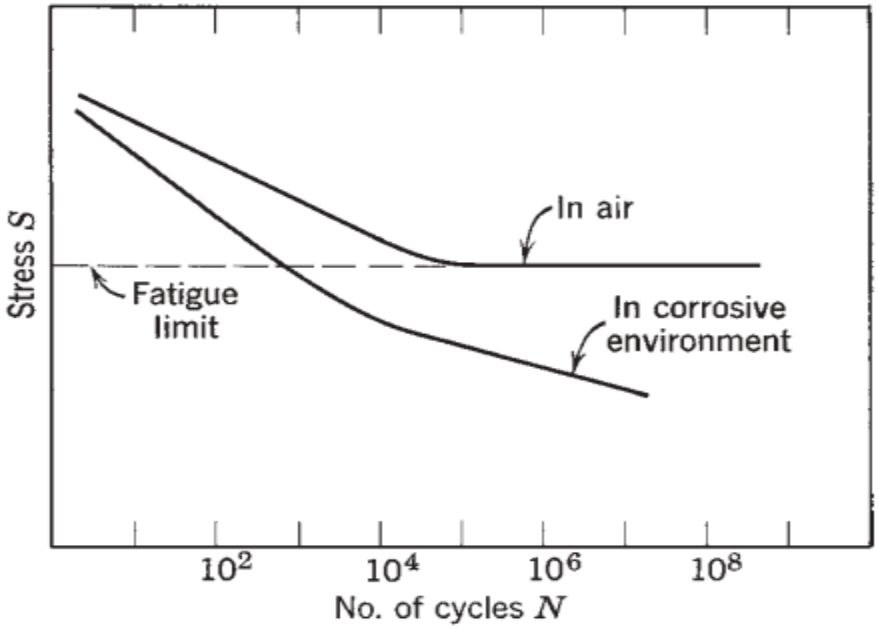

Figure 5: The effect of environment in fatigue limit and fatigue life of same material [45].

There are several methods to prevent corrosion fatigue in a structural material such as surface finishing, careful grinding, modifying rough surfaces after casting and

forging, avoiding unnecessary notches and dents and applying protection coating [20]. In industries, while manufacturing the materials they use different techniques helps preventing corrosion fatigue such as inducing compressive residual stresses in structural components using Shot Peening, Laser peening, or Low Plasticity Burnishing [37].

2.4 Fracture Mechanics

Fracture mechanics can be defined as the technique of minimizing the possibility of fracture on cracked material [33]. Fracture mechanics focus on studying the material properties that related to component behavior and give the data that helps in selecting the materials to minimize the possibility of failure due to cracks [33].

As fracture mechanics deals with cracks, understanding the behavior of crack growth is important as well as the type of loading that a crack can experience [5]. Figure 6 shows the three displacement modes as a result of the loading type that cracked structure experience.

- Mode I: known as Opening mode, where crack faces move apart due to tensile stress that acts normal to the crack plane.
- Mode II: known as Sliding mode, where crack faces slide due to shearing stress that acts parallel to crack plane and perpendicular to the crack front.
- Mode III: known as Tearing mode, where crack faces slide due shearing stress that act parallel to crack plane and parallel to the crack front [33].

A cracked body can experience one of these displacement modes or a combined of them [5]. However, as this study has been conducted with tension-tension stresses, mode I and mode II are the types of displacement modes that cracks experience.

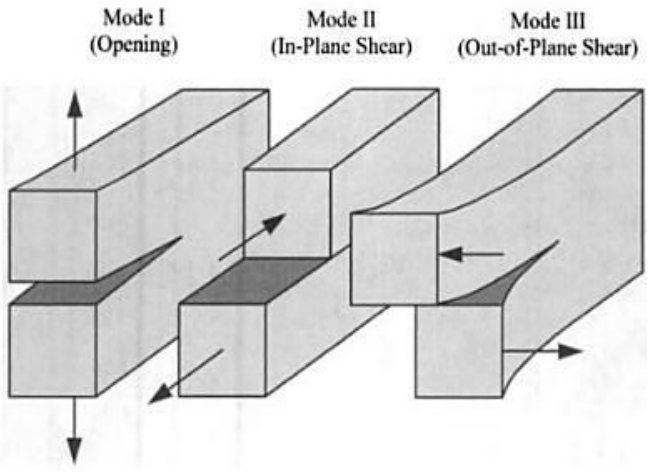

Figure 6: Three modes of crack displacement [5].

In this study, the cracks propagated from a circular hole in a thin cruciform specimen under biaxial loading, after being notched and then precracked. Thus, to better understand the propagation of crack, originating from a circular hole, and also to understand the direction of the propagation, the following sections will provide a literature review on the stress intensity factors for crack initiated from a circular hole, stress transformation, global and local coordinate systems and direction of crack propagation, including an analytical approach to predict the direction of crack propagation.

2.4.1 Stress Intensity Factors for a Crack Originating from a Circular Hole in Thin Plate under Biaxial Loading

The stress intensity factor is the magnitude of stresses near the tip of crack [33]. In case of mode I loading the stress are depending on r and θ as follows [33]:

$$\sigma_x = \frac{K_I}{\sqrt{2\pi r}} \cos\frac{\theta}{2}\left[1 - \sin\frac{\theta}{2}\sin\frac{3\theta}{2}\right] + \cdots \quad (2.1)$$

$$\sigma_y = \frac{K_I}{\sqrt{2\pi r}} \cos\frac{\theta}{2}\left[1 + \sin\frac{\theta}{2}\sin\frac{3\theta}{2}\right] + \cdots \quad (2.2)$$

$$\tau_{xy} = \frac{K_I}{\sqrt{2\pi r}} \cos\frac{\theta}{2}\sin\frac{\theta}{2}\cos\frac{3\theta}{2} + \cdots \quad (2.3)$$

$$\sigma_z = \tau_{xz} = \tau_{yz} = 0 \text{ (for plane stress condition)} \quad (2.4)$$

But in this study, in-plane biaxial loading is applied to thin cruciform specimen, and plane stresses conditions applied to crack originated from notched circular hole in presence of mode I and mode II. The stress intensity factor can be expressed by [19]:

$$K_I = \frac{\sqrt{\pi r}}{2\sqrt{2}} \sqrt{\frac{l_0\,(l_0 + 2)^3}{(l_0 + 1)^3}}\,(S_{yy} + S_{xx} - (S_{yy} - S_{xx})\cos 2\alpha) \quad (2.5)$$

and

$$K_{II} = \frac{\sqrt{\pi r}}{2\sqrt{2}} \sqrt{\frac{l_0\,(l_0 + 2)^3}{(l_0 + 1)^3}}\,(S_{xx} - S_{yy})\,\sin 2\alpha\,) \tag{2.6}$$

where l_0

$$l_0 = \frac{1}{2}\left(-1 + \frac{a}{r} + \sqrt{2\frac{a}{r} + \frac{a^2}{r^2} + 1}\right) \tag{2.7}$$

where:

S_{xx} is the stress in x-direction (N/m^2).

S_{yy} is the stress at in y-direction (N/m^2).

r is the radius of the circular hole (m).

a is the length of the crack (m).

α is the angle between the y-axis and the crack.

φ is the angle between the x-axis and the crack ($\varphi = \frac{\pi}{2} - \alpha$).

Figure 7 show cracked circular hole subjected to biaxial stresses.

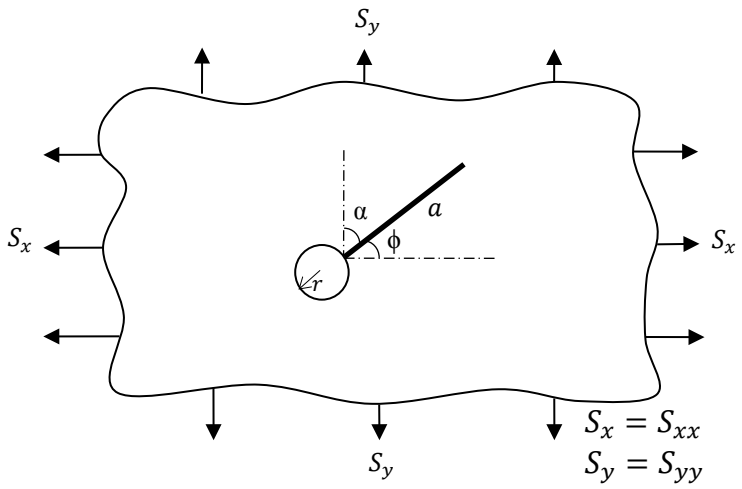

Figure 7: Cracked circular hole subjected to biaxial stresses.

In this study, the circular hole is notched at φ =45°, the crack propagates and grows at φ =45° which simplify equation (2.5) and (2.6) to become [19]:

$$K_I = \frac{\sqrt{\pi r}}{2\sqrt{2}} \sqrt{\frac{l_0\,(l_0 + 2)^3}{(l_0 + 1)^3}}\,(S_{yy} + S_{xx}) \tag{2.8}$$

and

$$K_{II} = \frac{\sqrt{\pi r}}{2\sqrt{2}} \sqrt{\frac{l_0\,(l_0 + 2)^3}{(l_0 + 1)^3}}\,(S_{yy} - S_{xx}) \tag{2.9}$$

2.4.2 Cyclic Loading

Cyclic loading is defined as the function of repeated or fluctuating loads in specific location at the structural component. There are basic definitions descript the relation between those loads or stresses. The stress range ($\Delta\sigma$) is the difference between the maximum stress and the minimum stress [33]. The mean stress, (σ_m) is the average between the maximum and the minimum stress and the stress amplitude or alternating stress (σ_a) is the half of the stress range and it can be zero but in our case it is not. And those definitions can be mathematically expressed as [33]:

$$\Delta\sigma = \sigma_{max} - \sigma_{min} \tag{2.10}$$

$$\sigma_a = \frac{\Delta\sigma}{2} = \frac{\sigma_{max} - \sigma_{min}}{2} = \frac{\sigma_{max}}{2}(1 - R) \tag{2.11}$$

$$\sigma_m = \frac{\sigma_{max} + \sigma_{min}}{2} \tag{2.12}$$

The stress ratio R is the ratio that describe the type of cyclic loading and it is mathematically expressed as:

$$R = \frac{\sigma_{min}}{\sigma_{max}} \tag{2.13}$$

When R=0 that means it is repeated in one direction stress cycling, when R= -1 it is completely reversed cycling and when R is varying from 0 to 1, it is describing the tension-to-tension cycling [33].

2.4.3 Effect of R- ratio on Fatigue Crack Growth

R-ratio is known as ratio stress and it is a ratio where minimum stress divided into maximum stress and mathematically expressed as:

$$R = \frac{\sigma_{min}}{\sigma_{max}} = \frac{\Delta K_{min}}{\Delta K_{max}} \tag{2.14}$$

In fact, an increase in the R-ratio of a cyclic loading causes growth rates for a given ΔK to be larger [33]. And the effect is usually more for more brittle materials but in highly ductile, weak R effect is observed [33].

In this work Walker equation is used to describe the effective of R-ratio for crack propagation and fatigue failure and it is good explanation of the effect of R on da/dN vs ΔK curves. Walker expressed $\overline{\Delta\sigma}$ in terms of stress ranges and stress ratio [33].

$$\overline{\Delta\sigma} = \frac{\Delta\sigma}{(1-R)^{(1-\gamma)}} \tag{2.15}$$

In term of stress intensity factor range equation (2.15) becomes

$$\overline{\Delta K} = \frac{\Delta K}{(1-R)^{(1-\gamma)}}$$

(2.16)

Where

$\overline{\Delta K}$ is the stress intensity factor range at zero to tension (R=0).

γ is a constant for a material.

From Paul Paris equation lets donate constant C to be C_0 for special case R=0.

$$\frac{da}{dN} = C_0(\Delta K)^m \quad (2.17)$$

Since ΔK is an equivalent for $\overline{\Delta K}$ for R=0, substitute $\overline{\Delta K}$ for ΔK in eq. 2.17:

$$\frac{da}{dN} = C_0(\frac{\Delta K}{(1-R)^{(1-\gamma)}})^m \quad (2.18)$$

As γ is a constant for a material and it describe the effect of R-ratio in da/dN vs ΔK curves and it has been calculated in this study for 7075-T6 aluminum alloy at air and corrosive environment and that will be clear in result chapter.

2.5 Previous Research

The corrosion fatigue failure has been studied experimentally for different types of materials, and that explain the failure behavior of these materials due to combined effect of corrosion and fatigue. Paris and McEvily stablished the foundations of crack growth rate study in 1985. McEvily studied the crack growth of aluminum alloys 7075-T6 and 2024-T3 using fatigue testing machine [24]. Paris studied crack growth rate and he was the first one studying the stress intensity factor range (ΔK) versus the crack

propagation rate (da/dN), Paris law determine the crack growth rate per loading cycle using the load ratio and stress intensity ranges [21].

Lately, many studies have been investigating the crack propagation and the environmental effects on crack growth behavior, many kinds of research carried out in different aspects using advanced technology. The data from those studies documented and available but when it comes to aerospace field the concept changes because these studies had been conducted under uniaxial fatigue conditions, aircrafts faces Mixed mode of stresses through the flight and that limits the benefits of data conducted from uniaxial fatigue tests [5,9,26]. Recently, all researchers focus on multi-stresses and they started using biaxial fatigue test machines to determine the crack growth behavior under the in-plane biaxial loading condition and the studies conducted in two types of environments ambient air and the saltwater (3.5%) environment, using cruciform-type specimens of aircrafts grade aluminum alloy series. In these studies they used a fracture mechanics approach. Mains studies of fatigue crack growth behavior under the in-plane biaxial loading condition and results in details are analyzed below.

Liu and Dittmer [23] studied the behavior of the fatigue crack growth of center-cracked cruciform specimens of 7075-T7351 and 2024-T351 aluminum alloys with different biaxial stress ratios under biaxial loading conditions. The results are the crack will grow in a straight line when the stress component normal to the crack direction is greater than the stress component parallel to the crack direction, and the larger biaxial stress component controls the crack growth rate and depends on the biaxiality ratio. The effect of stress parallel to the crack on crack growth rate is negligible.

Hopper and Miller [17] used a servo-hydraulic testing machine in a circular notched and un-notched plates under biaxial stresses to study the propagation of the fatigue cracks. The machine was unable to run the horizontal and vertical components of stresses at the same time. So they run the test by keeping the horizontal stress fixed while cycling the vertical stress component with λ = -1, 0 and 1. They calculated the number of cycles to determine the crack growth rate and they used microscope and curve-fitting technique to measure crack length. The result was the compressive loading increases the crack growth rates while the tensile loading deceases it.

Anderson and Garrett [4] studied the effect of biaxial stress on the crack growth on steel cruciform specimens with central crack. They compared uniaxial and biaxial loading after changing the biaxialty ratio. The result was received that the crack growth rate in biaxial loading with tensile stress parallel to the crack is lower than the crack growth rate in uniaxial loading while the crack growth rate in biaxial loading with compressive stress parallel to the crack is higher than the crack growth rate in uniaxial loading.

Sunder and Ilchenko studied the fatigue crack growth in internal cabin to find the effect of mixed mode of pressure and gust loading in internal cabin by applying biaxial quasi-static load in a laboratory environment with constant amplitude. Two materials had been studied with different thickness, first specimen was made of steel with 1 mm thickness, second specimen was 2024-T3 aluminum alloy with 2.7 mm thickness. They found that the fatigue crack growth rate is sensitive to biaxial stresses [42].

Shanyavskiy conducted fatigue crack growth experiments for cruciform specimens made from AK4-1T1 and D16T Al-alloy with thickness range of 1.2 to 10 mm under biaxial cyclic loadings to find the effect of crack closure under plane-stress condition, plane-strain condition and out-of phase loading condition [38]. The study had been done under constant and variable amplitude of cyclic loads with different biaxiality ratios and stress ratio. The biaxility ratio was from -1.4 to 1.5, and the stress ratio range from 0.05 to 0.8. The result was that the plastic zone increased with the increase of phase difference from 0° to 180°, and it decreased with further increasing of the phase difference [38]. Fatigue cracks grow faster as biaxiality stress ratios increase [38].

Lee and Taylor [22] examined aluminum alloys 1100-H14 and 7075-T651 cruciform specimens of 2mm thickness, with a horizontal or a 45° inclined center notch to study the effect of biaxial stresses on the fatigue life, fatigue crack growth and path. The test was conducted by subjecting these specimens to in-phase or out-of-phase biaxial load with biaxiality ratio λ from 0 to 1.5 and stress ratio R= 0.1 and loading frequency 15 Hz in air environment. The result was that at a given biaxial stress ratio the fatigue life increases for in-phase and out-of-phase loading as longitudinal stress decreases and he noticed that fatigue life while applying in-phase loading is much better than the fatigue life while applying out-of-phase loading. Also, there is a noticeable decrease of crack growth rate and increase in fatigue life for high biaxial stress ratio under in-phase loading comparing to tiny change with change in biaxial stress ratio under out-of-phase loading. He found also that the path of fatigue crack is sensitive to initial center notch location, phase angle and biaxial stress ratio.

Yuuki et al. [48] also studied the effect of biaxial stresses on the fatigue crack growth on cruciform specimens made of SUS 304 stainless steel using biaxial fatigue testing machine. For center cracks, they tried to determine the stress intensity factor with constant and changing biaxial stress condition tests. The specimen was tested under biaxiality ratio of -1, 0, and 1 and stress ratio of 0.1. They used a travelling microscope to measure the crack length. The results were that at low stress level the biaxiality had negligible effect on crack growth rates, but noticeable effect at high stress levels [48].

At AFIT many research has been done by Mall, Misak, Perel and Sabelkin. They studied fatigue crack growth behavior under biaxial cyclic loadings in air and saltwater (3.5% NaCl) environments with biaxiality ratios, λ=1 and 1.5 and stress ratio was R=0.5. Cruciform specimens made from aluminum alloy 7075-T6 were used in the experiments. Specimen geometry that has been used in all of the experiments was 3.18 mm thickness, a center hole of 6 mm diameter with a machined notch of a 1 mm long and 0.25 mm wide at an angle 45° to horizontal and vertical arms [28, 29]. All experiments start with making pre-crack of 1mm from the notch under biaxial fatigue loading condition, the notch and the crack are perpendicular to the rolling direction of the specimen [28, 29]. An optical microscope system was used to measure the crack length. For analyzing the data from the experiments and to calculate the stress intensity factors on points along the crack propagation rate (da/dN) the ABAQUS finite element analysis program was used. In the same way, the uniaxial fatigue crack growth experiments were conducted and the comparison between biaxial and uniaxial loading in crack initiation were made. The crack initiation starts under a lower driving force level for biaxial fatigue comparing to

uniaxial fatigue [28]. The authors found that the crack initiation driving force decreases with increase of biaxial stress ratio [28]. Also, crack initiation and growth was found coplanar with the notch under $\lambda = 1$ and non-coplanar with the notch under $\lambda = 1.5$ [28]. In air environment, crack growth rate for biaxial fatigue with $\lambda = 1$ is equal to crack growth rate for the uniaxial fatigue ($\lambda = 0$), but it was faster under biaxial fatigue with $\lambda = 1.5$ for a given crack driving force [28]. In saltwater environment, crack growth rate under uniaxial fatigue was the slowest and it was increased by increasing biaxial stress ratio for a given crack driving force [27]. They found for fatigue damage mechanisms that fatigue crack propagation was planar slip when $\lambda = 0$, wavy slip when $\lambda = 1.5$ but a combination of the two when $\lambda = 1$ in air environment [27]. Fatigue crack propagation was transgranular for uniaxial and biaxial fatigue with $\lambda = 1$ in saltwater environment [27].

2.6 Why This Thesis?

Much is known about fatigue crack growth under uniaxial loading conditions, but there is a limited number of studies under biaxial loading conditions. These studies have shown that biaxial fatigue has an effect on the crack growth rate. Some of these studies had addressed the in-phase or out-of-phase loading conditions [38]. All of these studies had been conducted with constant value of stress ratio R=0.5 and none of them studied the effect of changing stress ratio on fatigue crack growth behavior of a material that is subjected to biaxial loading in air and saltwater environments. The present research is a unique study where the fatigue crack growth behavior of specimen made of 7075-T6 aluminum alloy was inspected under in-plane biaxial loading in both air and saltwater

(3.5% NaCl) environments for wide range of R-ratio, R=0.1, 0.5 and 0.7. In addition, the test generates more accurate definition of Walker equation parameters and leads to more accurate prediction of fatigue crack growth rate at different stress ratio. This research presents the details and the results of this experimental work.

III. Methodology

3.1 Material

Aluminum alloy 7075-T6 is the material that is used in this research. The alloy is a very high strength material used in highly stressed structure. Besides of its strength it

has good properties that make it applicable for aerospace applications. Table 1 and Table 2 shows the chemical composition and mechanical properties of AA 7075-T6 [3].

Table 1:Chemical compositions of AA7075-T6 alloy [3].

Element	**Weight Percentage**
Aluminum	87.1 - 91.4
Zinc	5.1-6.1
Magnesium	2.1-2.9
Copper	1.2-2
Iron	Max 0.5
Silicon	Max 0.4
Manganese	Max 0.3
Chromium	0.18-0.28
Titanium	Max 0.2
Other	each Max 0.05
Other	total Max 0.15

7075-T6 aluminum alloy is one of 7000 aluminum series where is zinc is the principle alloying with other elements such as copper, magnesium and chromium. 7000 aluminum series considered as the strongest aluminum alloy and it has the sufficient properties such as high strength, low density, good fatigue strength, toughness and corrosion resistance to be used in aircraft structural components and other high-strength applications [3,1]. T6 indicates that the material is solution heat treated and artificially aged and that has been done by homogenizing the cast 7075 at 450 °C for several hours,

followed by aging at 120 °C for 24 hours and such a good treatment make AA 7075-T6 one of the most common alloys used in the aircraft structures [3].

Table 2: Mechanical properties of AA 7075-T6 [3].

Mechanical Properties			
	Metric	English	Comments
Hardness, Brinell	150	150	AA; Typical; 500 g load; 10 mm ball
Hardness, Knoop	191	191	Converted from Brinell Hardness Value
Ultimate Tensile Strength	572 MPa	83000 psi	AA; Typical
Tensile Yield Strength	503 MPa	73000 psi	AA; Typical
Elongation at Break	11 %	11 %	AA; Typical; 1/16 in. (1.6 mm) Thickness
Modulus of Elasticity	71.7 GPa	10400 ksi	AA; Typical; Average of tension and compression. Compression modulus is about 2% greater than tensile modulus.
Poisson's Ratio	0.33	0.33	
Fatigue Strength	159 MPa	23000 psi	AA; 500,000,000 cycles completely reversed stress;
Fracture Toughness	20 MPa-m½	18.2 ksi-in½	K(IC) in S-L Direction
Fracture Toughness	25 MPa-m½	22.8 ksi-in½	K(IC) in T-L Direction
Fracture Toughness	29 MPa-m½	26.4 ksi-in½	K(IC) in L-T Direction
Machinability	70 %	70 %	0-100 Scale of Aluminum Alloys
Shear Modulus	26.9 GPa	3900 ksi	
Shear Strength	331 MPa	48000 psi	AA; Typical
Density	2.81 g/cc	0.102 lb/in³	AA; Typical

3.2 Test Specimens

The test specimens used in this study was cruciform specimens machined from 7075-T6 aluminum alloy sheet. The geometry of the specimen 3.18 mm thickness with 120 mm length and a width of each arm of 45 mm, the radius of curvature at the junction of arms of 45 mm. All specimens had been drilled at the center with a hole of 6 mm diameter. A notch of 1 mm length and 0.25 mm width at an angle of 45° to horizontal and vertical arms was machined by electro-discharge method (EDM) to create stress concentration. After that, a precrack of 1 mm length under biaxial cyclic loading with biaxility ratio, $\lambda = 1$ with no phase difference was created from the machined notch. The pre-cracking was created for two reasons. Firstly, the notch of 0.25 mm width is not enough in order of measuring the initial stress intensity factor because the stress intensity factor is a characteristic of sharp crack. Secondly, to insure no defects in the specimen because the notch is the stress concentration and the crack supposed to start from it [5].

The applied maximum and minimum loads throughout the pre-cracking of the specimens were less than the loads used during the actual tests to avoid plasticity on crack tip. Figure 8 shows the experimental setup for biaxial loading along with the cruciform specimens. Cruciform specimens were cut in such a way that the notch and the precrack were perpendicular to the rolling direction. This gives possibility to compare our experiments with other results.

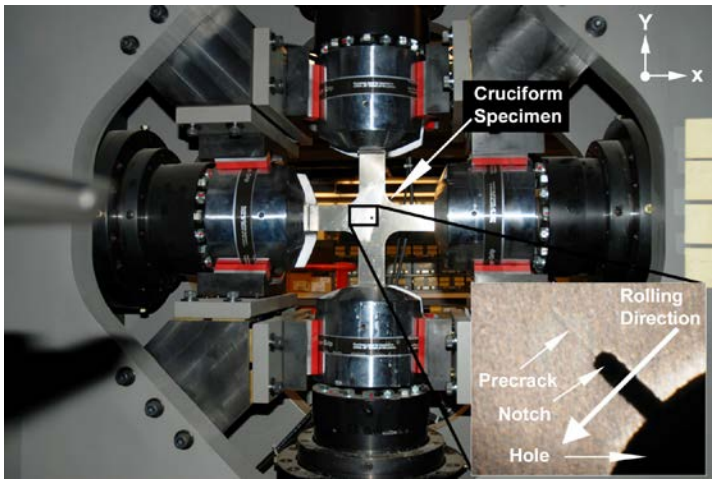

Figure 8: The biaxial experimental setup with a cruciform specimen.

3.3 Test Procedures

Material Testing System machine (MTS) is the machine used to perform the biaxial experiments. MTS has the ability to perform many test procedures like phase differences between applied loads change the maximum and the minimum loads in the horizontal and vertical directions for a desired stress ratio to study the closure effect for different stress ratios. In these experiments, the stress ratios for the horizontal and vertical loading were R_x=R_y=0.1, 0.5 and 0.7 respectively with biaxility ratio, $\lambda = 1$ with no phase difference. The frequency of both applied loads was 10 Hz.

In order to record the crack behavior after certain numbers of cycles, images of the crack were taken throughout the tests by using a PixeLINK camera having a resolution of 3 mega-pixels with an AF Micro Nikko 200 mm lens. The cycling process has been done until the crack reaches the failure length of about 20 mm. Figure 8 shows the experimental setup for biaxial loading along with the cruciform specimens.

The described above procedures had been done in laboratory air environment. In order to study the behavior of the crack under corrosion environment, a chamber with saltwater (3.5% NaCl) has been used in the experiments. Figure 9 shows the cruciform specimen with the attached saltwater chamber.

After conducting the tests, a software program called “uSCOPE” was used to measure the crack length at different number of cycles from the images which had been taken during the tests. This data used in drawing the crack in ABAQUS program.

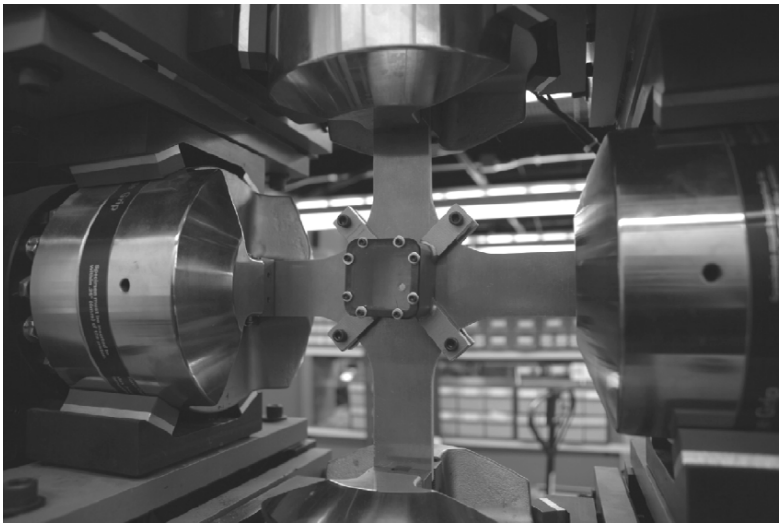

Figure 9: The cruciform specimen with attached saltwater chamber.

3.4 Finite Element Modeling

In order to address the stress ratio effect between the applied loads, a dynamic finite element analysis was carried out, using finite element program called Abaqus. stress intensity factor range (ΔK) were calculated.

The maximum and minimum external stresses, applied to the arms of the specimens, were calculated for each stress ratio in order to have same stress intensity range as shown below:

For stress ratio (R=0.1)

$$(S_x)_{max} = (S_x)_{max} = 7.96869 \times 10^7\ Pa \quad (3.1)$$

$$(S_x)_{min} = (S_x)_{min} = 7.96869 \times 10^6\ Pa \quad (3.2)$$

For stress ratio (R=0.5)

$$(S_x)_{max} = (S_x)_{max} = 1.0482 \times 10^8\ Pa \quad (3.3)$$

$$(S_x)_{min} = (S_x)_{min} = 5.2411 \times 10^7\ Pa \quad (3.4)$$

For stress ratio (R=0.7)

$$(S_x)_{max} = (S_x)_{max} = 1.5374 \times 10^8\ Pa \quad (3.5)$$

$$(S_x)_{min} = (S_x)_{min} = 1.0762 \times 10^8\ Pa \quad (3.6)$$

After conducting the experiments in laboratory air and saltwater (3.5% NaCl) environments, Abaqus was used to calculate the stress intensity factors in points at different number of cycles in order to address the fatigue crack growth curve along the crack propagation rate (da/dN) of the test specimens. To generate more accurate definition of Walker equation parameters and have more accurate prediction of fatigue crack growth rate at different stress ratio, the fatigue crack growth rate data obtained

from the experiments at three stress ratios are used to determine the parameters of the Walker equation:

1. Determining m

   From equation (2.17) C and m are the Paris's coefficient, so, by taking the average value of Paris exponent corresponding to different R-values m can be defined.

2. Determining C_0 and γ

   As Walker equation assumes that the same exponent m applies for all R-values, so two straight parallel lines for contrasting values of R formed on a log-log plot are sufficient to obtain approximate values of C_0 and γ

   By eliminating ΔK from equation (2.17) and (2.18) we will have two values of C in which the obey this equation

$$C = \frac{C_0}{(1-R)^{m(1-\gamma)}} \tag{3.7}$$

By eliminating C_0 from the two equations of C and taking logarithms of both sides for solving γ after that substituting γ back into either equations and solve for C_0.

IV. ABAQUS Program

ABAQUS is a software suite for finite element analysis originally released in 1978 by Dr. David Hibbitt, Dr. Bengt Karlsson and Dr. Paul Sorensen and it was known as ABAQUS Inc. In October 2005, Dassault Systèmes acquired ABAQUS Inc [46].

ABAQUS code consists of three products [46]:

- ABAQUS/Standard is a general-purpose, finite element module.
- ABAQUS/Explicit is an explicit dynamics finite element module.
- ABAQUS/CAE incorporates the analysis modules into a Complete ABAQUS Environment for modeling, managing, and monitoring ABAQUS analysis and visualizing results.

The finite element program was used in this research is ABAQUS/CAE, which is an intuitive and consistent user interface throughout the system. Figure 10 shows the main user interface when entering ABAQUS/CAE.

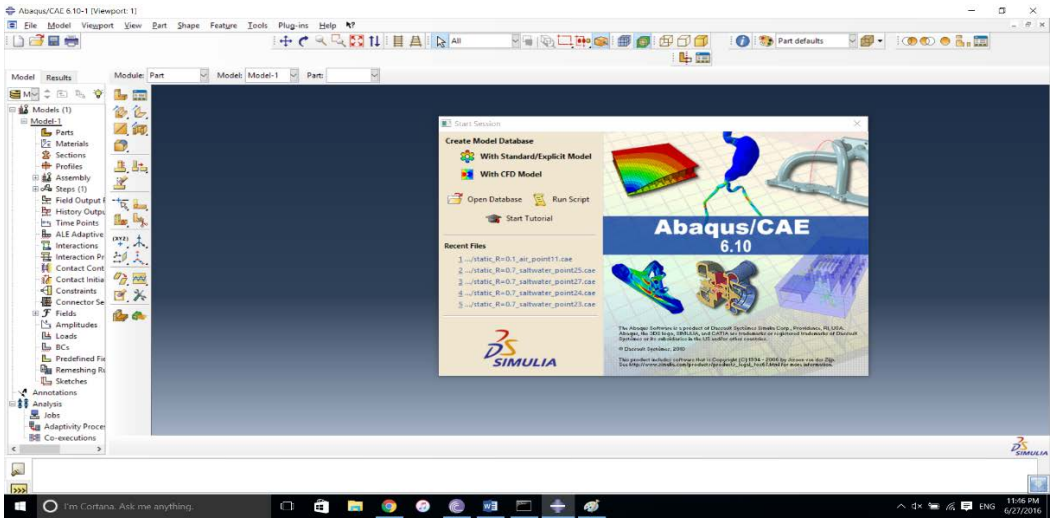

Figure 10: ABAQUS/CAE main user interface.

ABAQUS/Standard was used to calculate the stress intensity factors of the test specimens, and that have been done through the following steps:

1. The specimen was modeled with the same dimensions as the actual specimens used in the test. Figure 11 shows model of the specimen in ABAQUS.

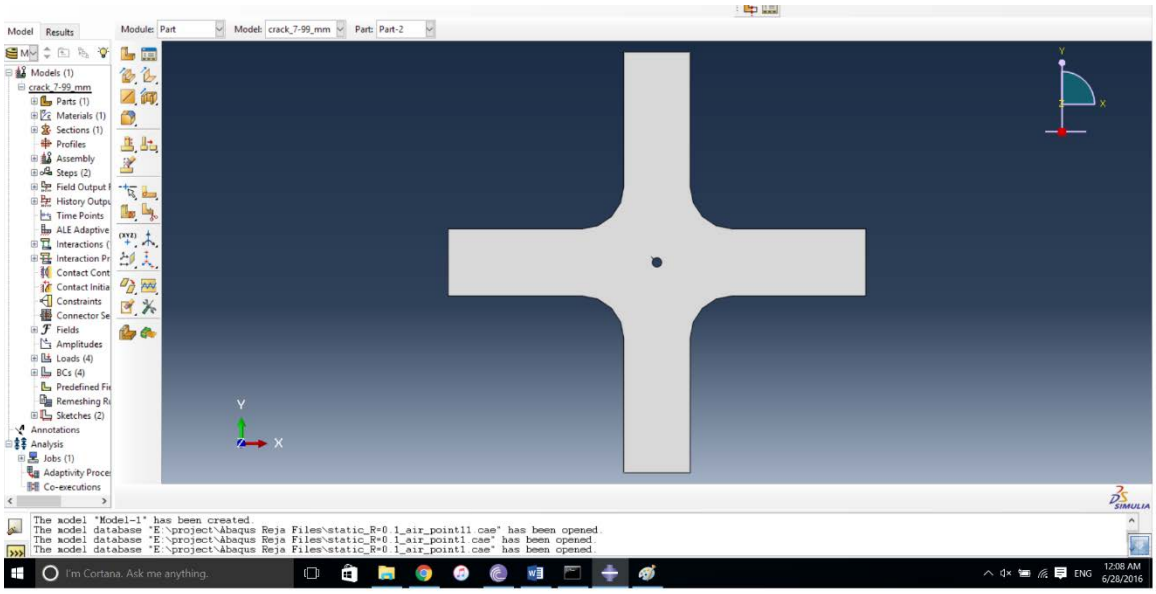

Figure 11: Model specimen in ABAQUS.

2. After modeling the specimens part and sketch section was used to redraw the changes in crack length for the new points.
3. In property section, the mechanical properties of the aluminum alloy were signed to the part (E=73 GPa, ν=0.33), where E is modulus of elasticity, ν is poisson's ratio.
4. In assembly section, the direction of the crack was specified to the tip of the crack with constrain set around the crack.

5. In step section, the required output of this run was selected to meet the study requirement.
6. In load section, the load was assigned to each arm of the specimen. This load changes with *R*-values changes.
7. In mesh section, a mesh was created for the whole specimen. Figure 12 shows close view of the generated mesh for one of the test specimen with crack length of 2mm.

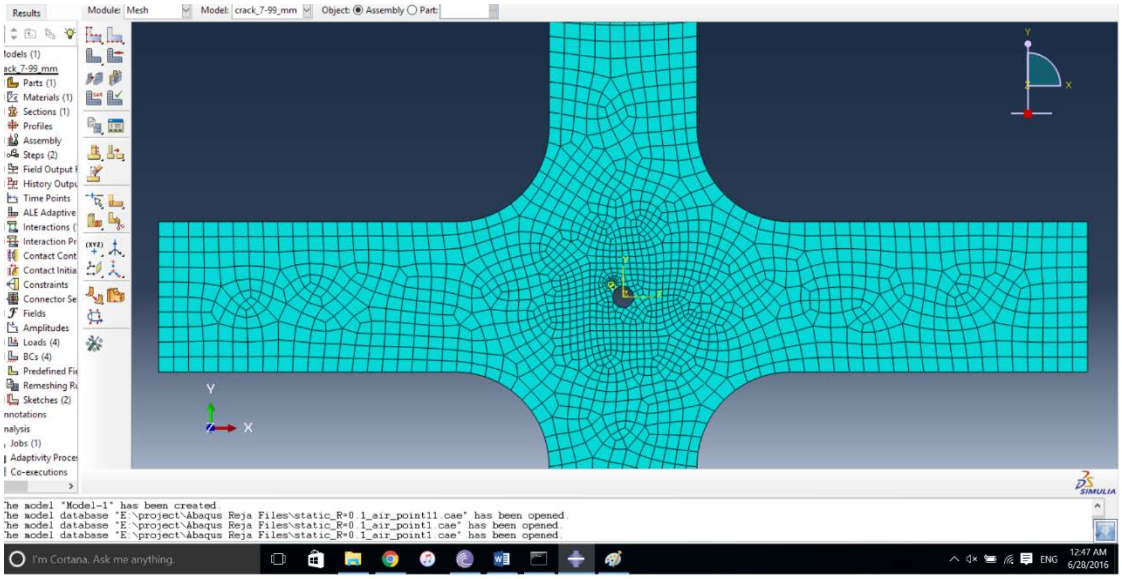

Figure 12: Close view of the mesh for 2 mm crack length specimen.

8. In job section, a job was created and submitted to run the model for the result output. Figure 13 shows the stress intensity factor data at one point along crack propagation rate.

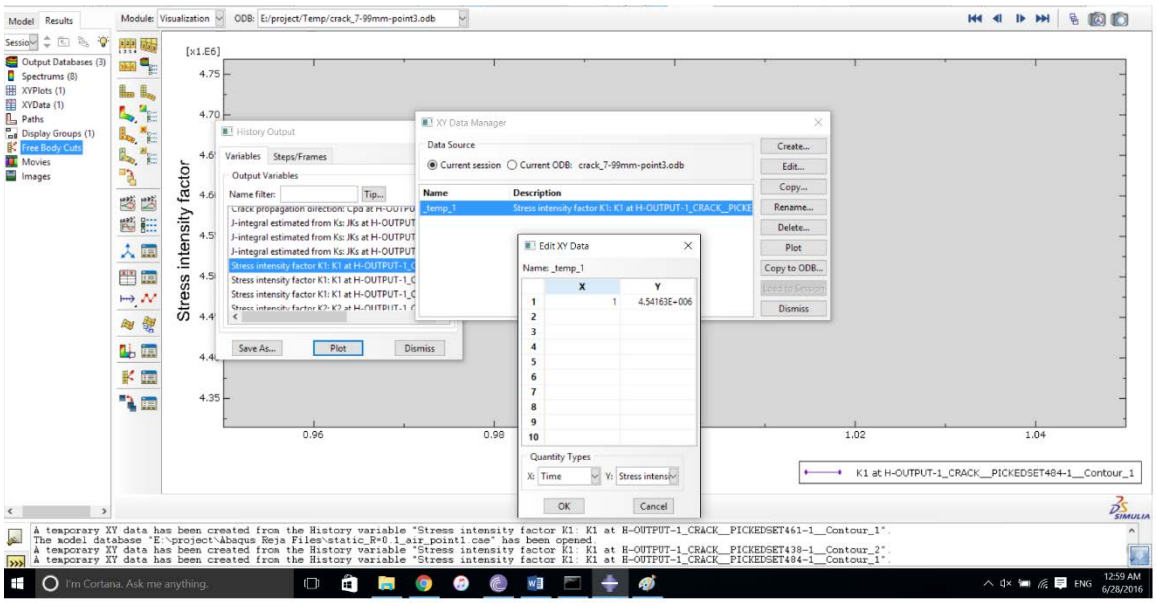

Figure 13: Stress intensity factor data at 2 mm crack length specimen at R=0.1.

Finally, the process was repeated for the increased crack length in order to find K_{max} as the cracks grow after certain number of cycles. For different *R*-values the procedure was the same but with the load is changed. Note that Abaqus shows the output as the K_{max} value [18]. The Δ*K* values must be calculated using this equation.

$$\Delta K = K_{max} * (1 - \mathrm{R}) \tag{4.1}$$

V. Results and Discussion

5.1 Overview

The chapter presents the result of all experiments that was conducted under in-plane biaxial loading in both ambient air and saltwater (3.5% NaCl) environments. As mentioned in the previous chapters, the fatigue crack growth behavior of specimens made from 7075-T6 aluminum alloy were tested with 0.1, 0.5 and 0.7 stress ratio.

Section 5.2 shows the crack path in air and saltwater environments. Section 5.3 presents the effect of stress ratio on fatigue crack growth rate in specimens tested under biaxial loads at different stress ratios in air and saltwater environments. Section 5.4 shows the effect of stress ratio on fatigue crack growth rate in specimens tested under biaxial loads in air and saltwater environments at constant stress ratio. Section 5.5 studies the fatigue crack growth rate data obtained from the experiments at three stress ratios to determine the parameters of the Walker equation. Table 3 shows a summary of the biaxial tests under fatigue loads with 0.1, 0.5, 0.7 stress ratio in air and saltwater environments.

Table 3:Summary of biaxial tests with 0.1 , 0.5 ,0.7 stress ratio in air and saltwater environments.

Environment	**Phase Difference (^{o})**	$R_{x,y}$	**λ**	**Frequency (Hz)**	**$F_{xy(max)}$ (N)**	**$F_{xy(min)}$ (N)**
Air	0	0.1	1	10	11000	1100
Air	0	0.5	1	10	15000	7500
Air	0	0.7	1	10	22000	15400
Saltwater	0	0.1	1	10	11000	1100
Saltwater	0	0.5	1	10	15000	7500
Saltwater	0	0.7	1	10	22000	15400

5.2 Crack Path

All specimens used in this research were biaxial cruciform specimens with a notch of 45° to the directions of the applied forces. The fatigue loads in vertical and horizontal directions were in-phase with biaxility ratio of $\lambda = 1$. The crack paths of all cases in air and saltwater were collinear with the notch. The crack grows along straight line of 45° to the directions of the applied forces. There is no effect of stress ratio on the crack path. Figure 14 shows the crack path of one of the specimens tested under biaxial loads in air environment and it is the same result for the specimens tested in saltwater environment.

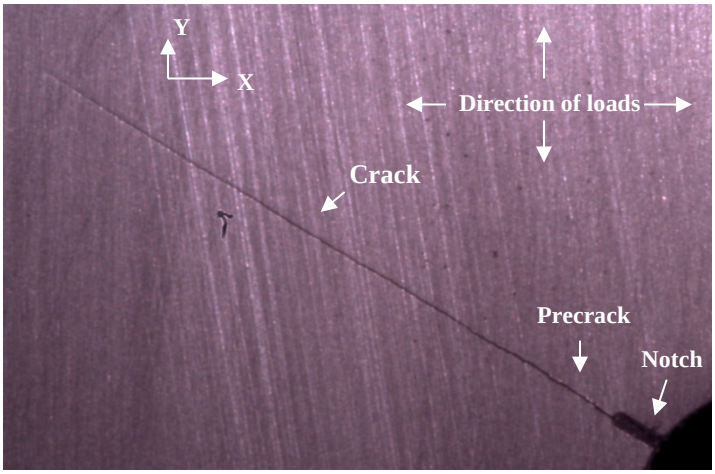

Figure 14: Typical crack path of one specimens tested under biaxial Loading in air environment.

5.3 Effect of Stress Ratio on Fatigue Crack Growth Rate

In order to study the effect of stress ratio on fatigue crack growth, a relationship between cyclic crack growth rate da/dN and stress intensity range ΔK should be present. The crack growth rate is obtained by plotting the crack length (a) versus the number of

cycles (N) for each specimens as shown in Appendix C Figure 61, Figure 62, Figure 63 and Figure 64 in excel and take the derivative of the slop equation in sake of finding fatigue crack growth rate *da/dN*. *da/dN* versus *ΔK* curves were obtained from the experimental data and they are shown in Figure 15 and Figure 16.

5.3.1 Effect of Stress Ratio on Fatigue Crack Growth Rate in Air Environment

Figure 15 shows the effect of stress ratio on the fatigue crack growth of 7075-T6 aluminum alloy in air environment. from the combined *da/dN* versus *ΔK* curves for R= (0.1, 0.5, 0.7) in air are shown. The fatigue crack growth rate at R=0.7 is higher than the fatigue crack growth rate at R=0.5 and the fatigue crack growth rate at R=0.5 is higher than the crack growth rate at R=0.1. Increase in the stress ratio leads to increase of fatigue crack growth rate for a given *ΔK*.

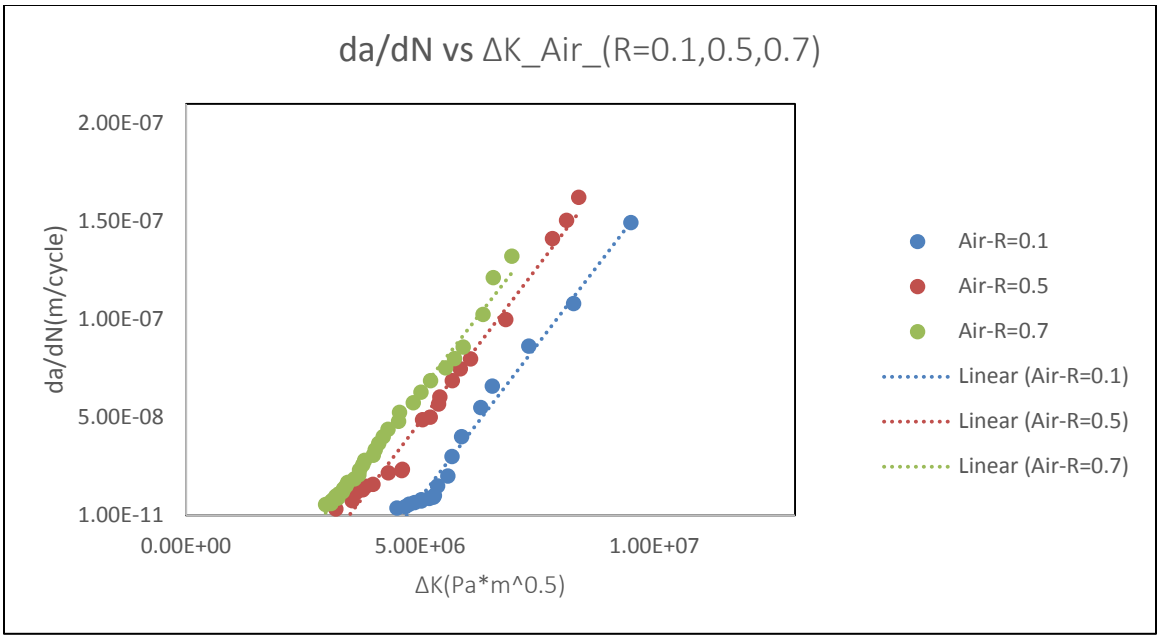

Figure 15: *da/dN* versus *ΔK* curves for R= 0.1, 0.5, 0.7 in air environment.

5.3.2 Effect of Stress Ratio on Fatigue Crack Growth Rate in Saltwater (3.5% NaCl) Environment

Figure 16 shows the effect of stress ratio on the fatigue crack growth of 7075-T6 aluminum alloy in saltwater (3.5% NaCl) environment. The combined *da/dN* versus *ΔK* curves for R= (0.1 ,0.5, 0.7) in saltwater (3.5% NaCl) are shown. The fatigue crack growth rate at R=0.7 is higher than the fatigue crack growth rate at R=0.5 and the fatigue crack growth rate at R=0.5 is higher than the crack growth rate at R=0.1. Increase in the stress ratio leads to increase of fatigue crack growth rate for a given *ΔK*.

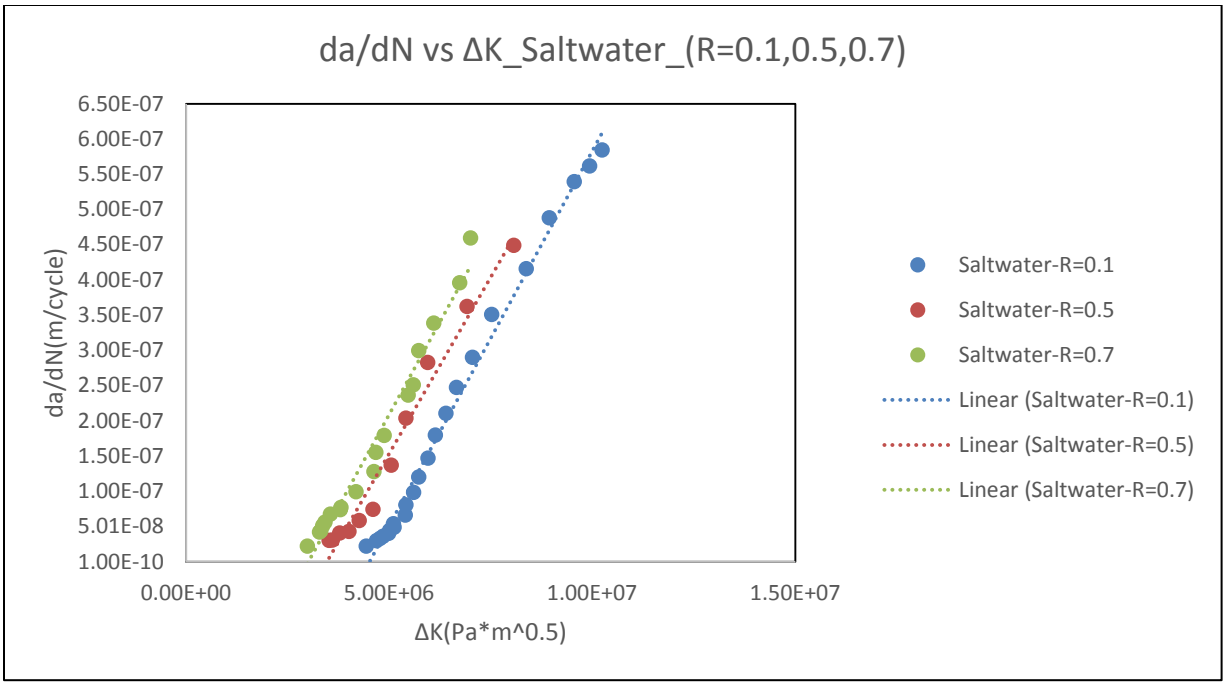

Figure 16: *da/dN* versus *ΔK* curves for R= 0.1, 0.5, 0.7 in saltwater environment.

5.4 Effect of Air and Saltwater (3.5% NaCl) Environment in Fatigue Crack Growth at Constant Stress Ratio

In this section, the fatigue crack growth curves in air and saltwater (3.5% NaCl) environments at stress ratio of (0.1, 0.5, 0.7) are compared to find the effect of environments. The result is as following:

- Figure 17 shows the companied fatigue crack growth in air and saltwater (3.5% NaCl) at R=0.1, the result was the fatigue crack growth in saltwater environment is higher than the one in air environment.

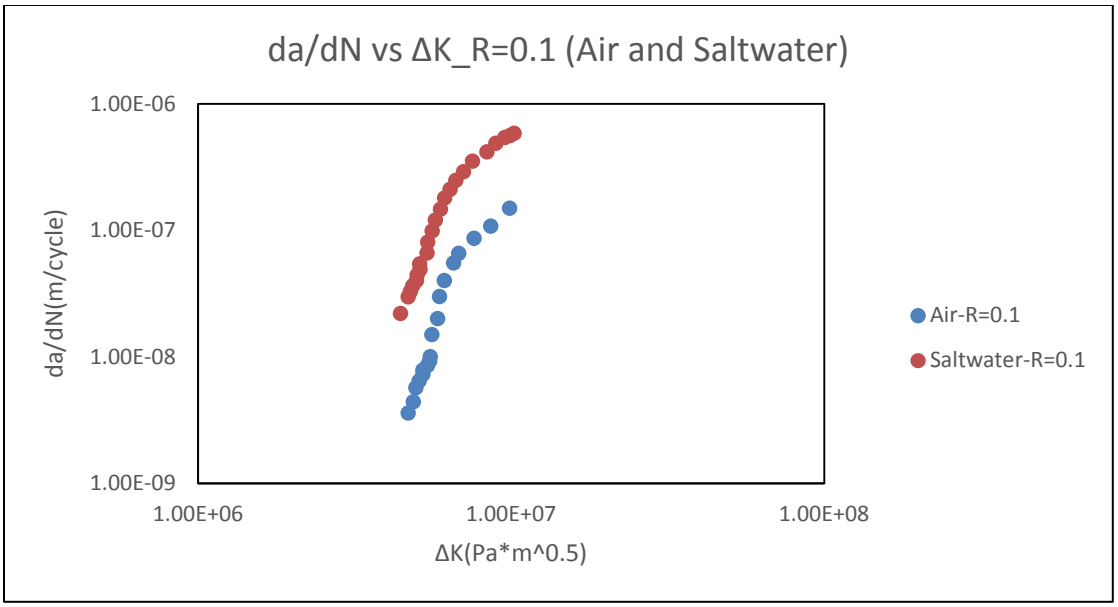

Figure 17: Fatigue crack growth rate in air and saltwater (3.5% NaCl) environments at R=0.1.

- Figure 18 shows the companied fatigue crack growth rate in air and saltwater (3.5% NaCl) environments at R=0.5. The result is that the fatigue crack growth in saltwater environment is higher than in air environment.

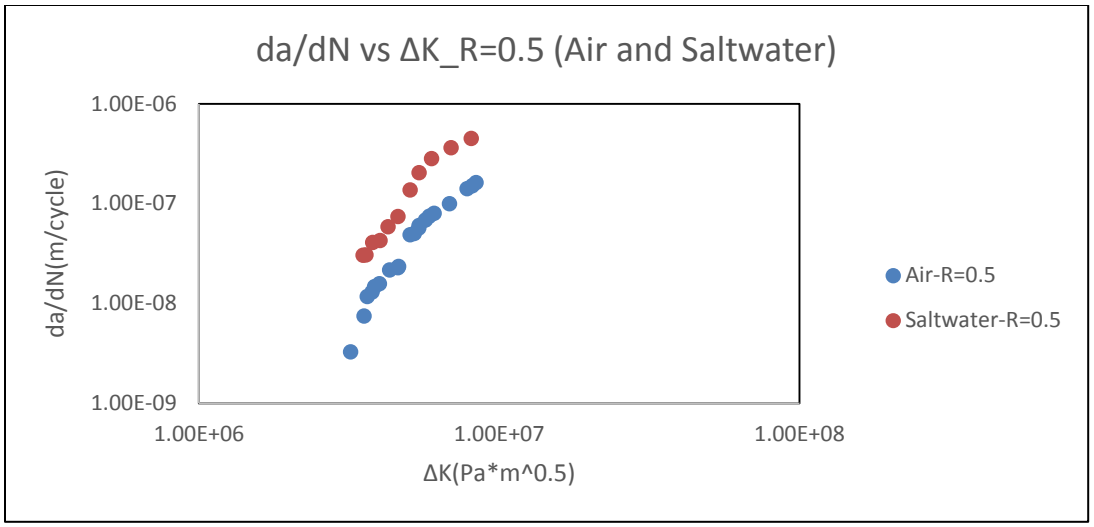

Figure 18: Fatigue crack growth rate in air and saltwater (3.5% NaCl) environments at R=0.5.

- Figure 19 shows the companied fatigue crack growth rate in air and saltwater (3.5% NaCl) environments at R=0.7. The fatigue crack growth rate in saltwater environment is higher than in air environment.

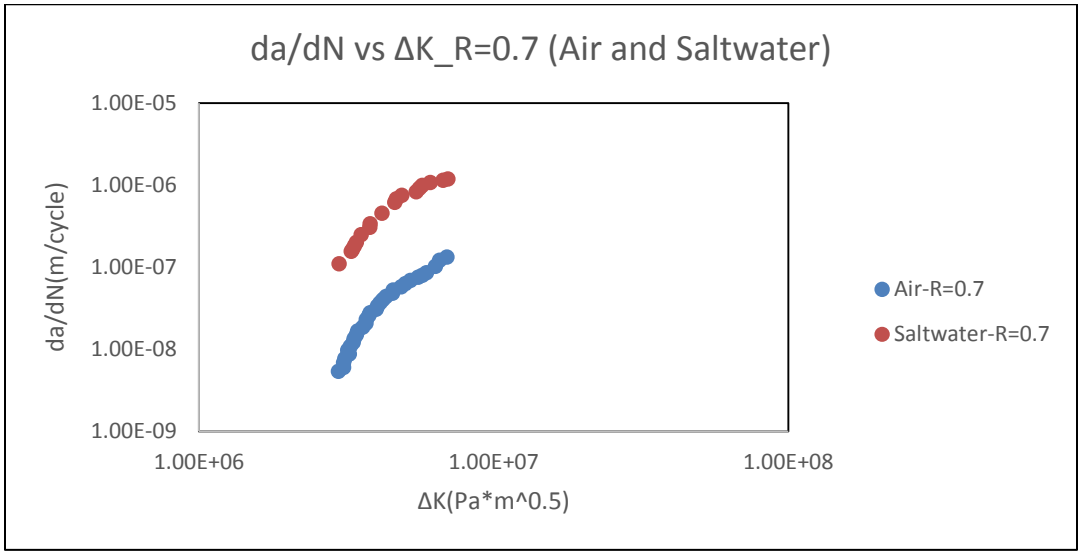

Figure 19: Fatigue crack growth rate in air and saltwater (3.5% NaCl) environments at R=0.7.

The fatigue crack is growing 50% faster in saltwater (3.5% NaCl) environment compared with air environment.

5.5 Parameters of Walker Equation to Predict Fatigue Crack Growth Rate at Different Stress Ratios

Walker equation as mentioned in Chapter 4 is used to predict fatigue crack growth rate at different stress ratios and it is based on test data and curve fitting. The method of calculating parameters of walker equation is discussed in Chapter 4. In addition, for applying Walker equation, the data of fatigue crack growth rate at (0.1, 0.5, 0.7) stress ratio should be collapsed onto a single curve. In order to determine parameters of Walker equation, logarithmic scale was used for fatigue crack growth rate of the cruciform specimens as a function of stress intensity factor for each experiment to determine Paris's coefficient (*C)* and Paris's exponent (*m)* for present experiments. Figure 20 and 21 shows fatigue crack growth in log-log scale for the present experiments.

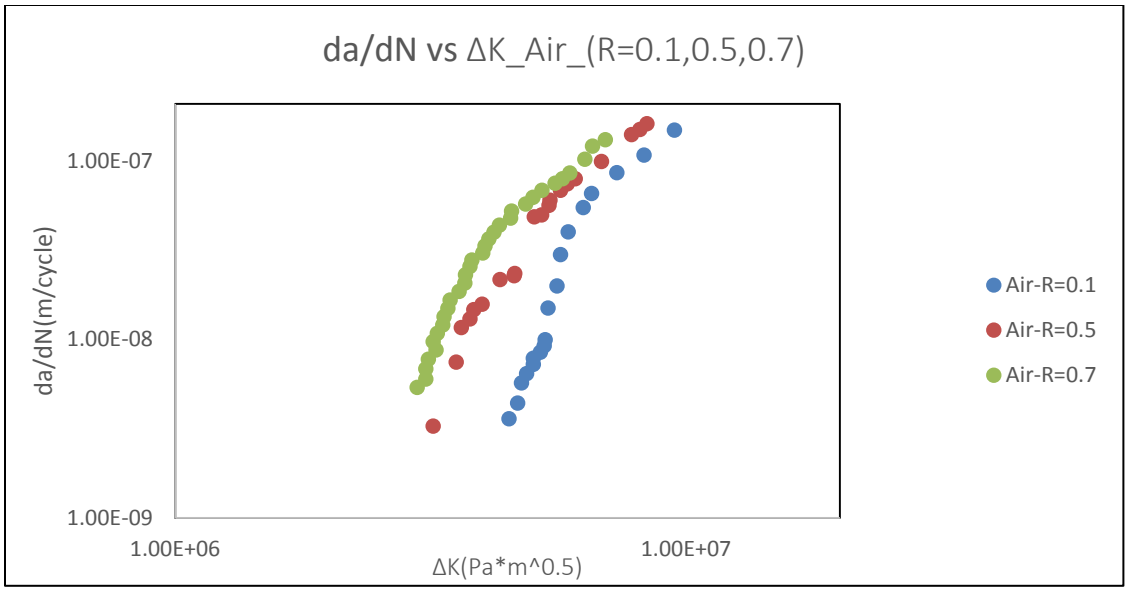

Figure 20: *da/dN* versus *ΔK* curves for R= 0.1 ,0.5 , 0.7 in air environment in log-log scale.

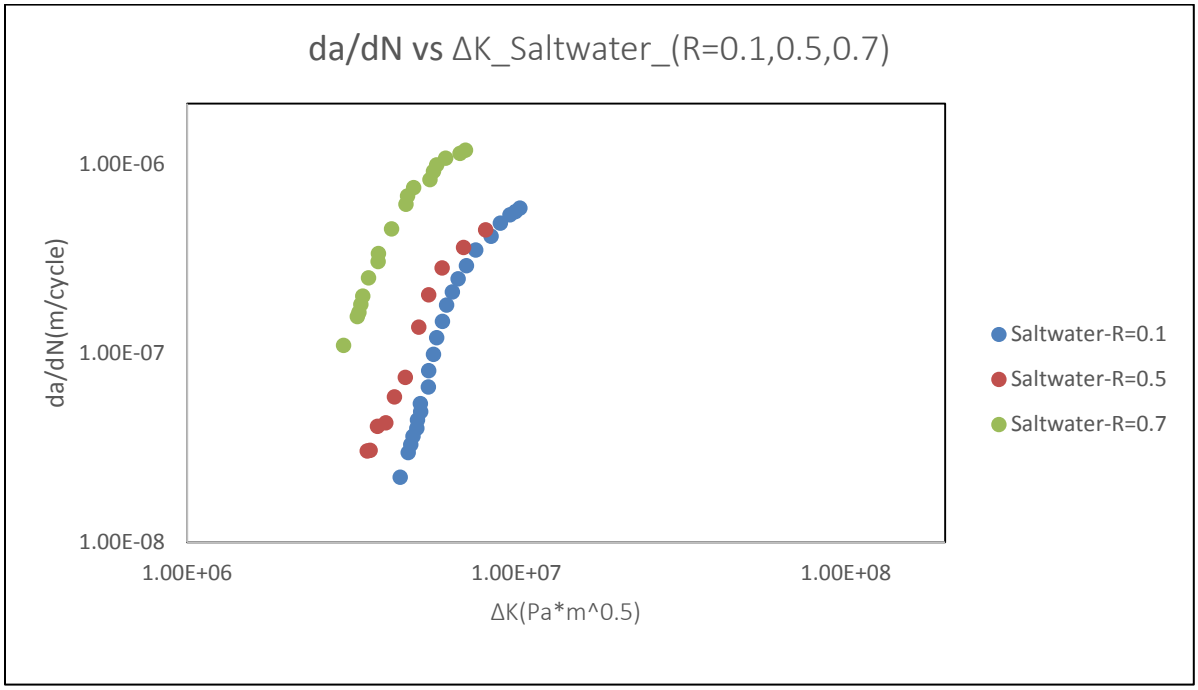

Figure 21: *da/dN* versus *ΔK* curves for R= 0.1 ,0.5 , 0.7 in saltwater environment in log-log scale .

Table 4 shows parameters of Walker equation that calculated using the experimental data. Figure 22 represented the data of the experiments in air environment by a single relationship based on Walker equation and that shows how much the effective fatigue crack growth rate predicted by Walker equation is very close to effective fatigue crack growth rates generated by the test in air environment. Similarly, Figure 23 shows the same in saltwater environment. Figure 24 shows the combination of test data of *da/dN* versus effective ΔK curves for R= 0.1 ,0.5 , 0.7 in air and saltwater environments and approximation with a single relationship based on Walker equation.

Table 4:Parameters of Walker Equation.

Environment	m	γ	C_0 **(m/cycle)**
Air	3.4	0.6	16×10^{-32}
Saltwater	3.3	0.7	4.5×10^{-30}

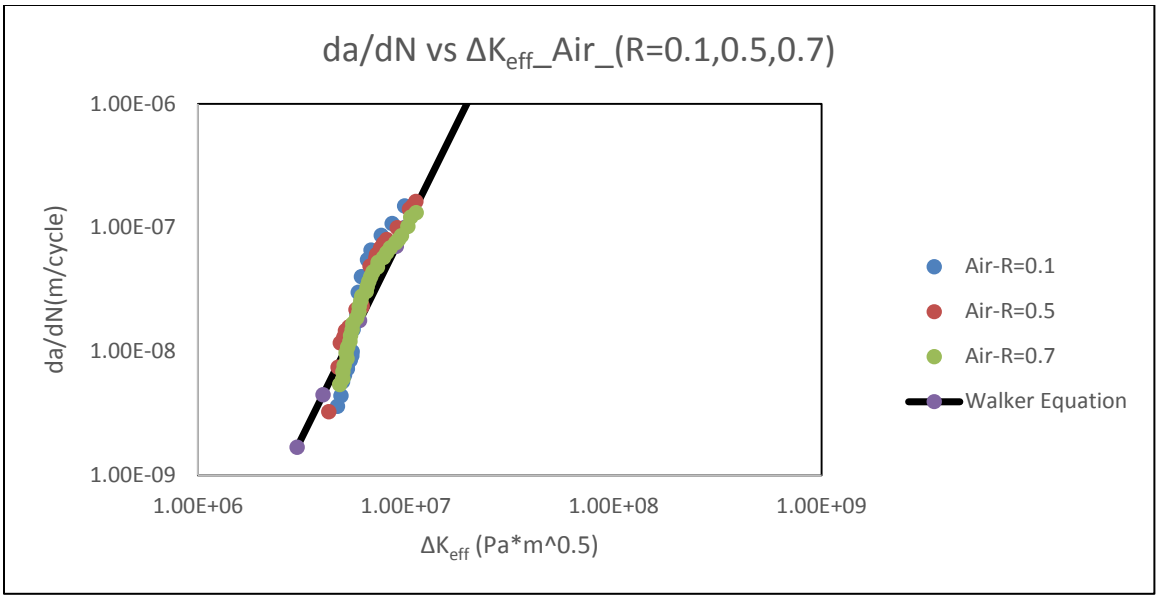

Figure 22: Combination of test data of *da/dN* versus effective *ΔK* curves for R= 0.1 ,0.5 , 0.7 in air environment and approximation with a single relationship based on Walker equation.

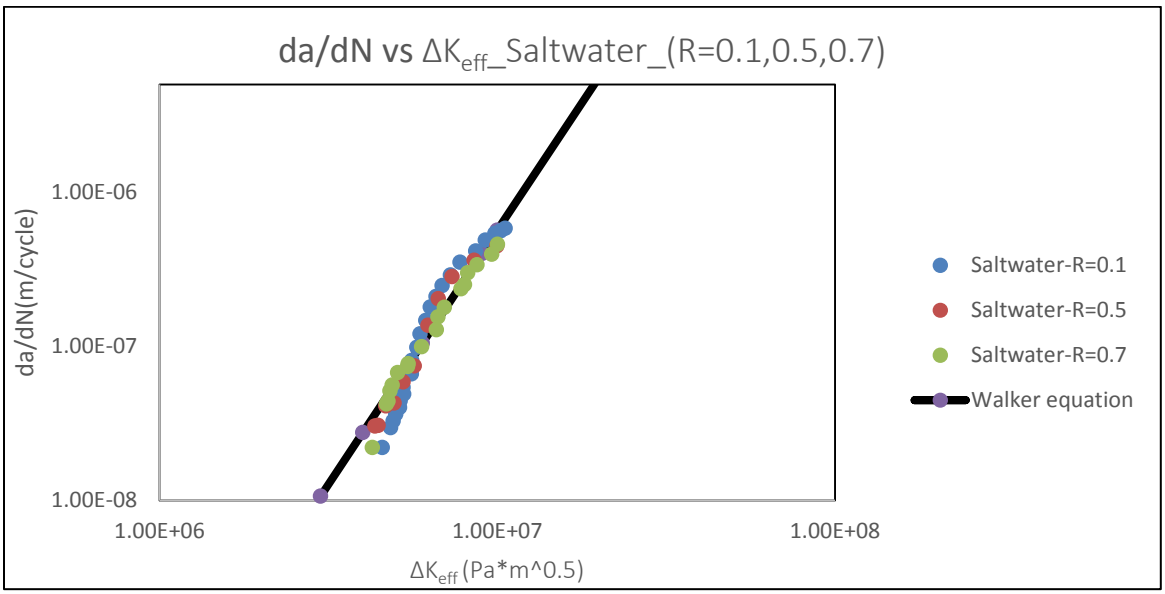

Figure 23: Combination of test data of *da/dN* versus effective *ΔK* curves for R= 0.1 ,0.5 , 0.7 in saltwater environment and approximation with a single relationship based on Walker equation.

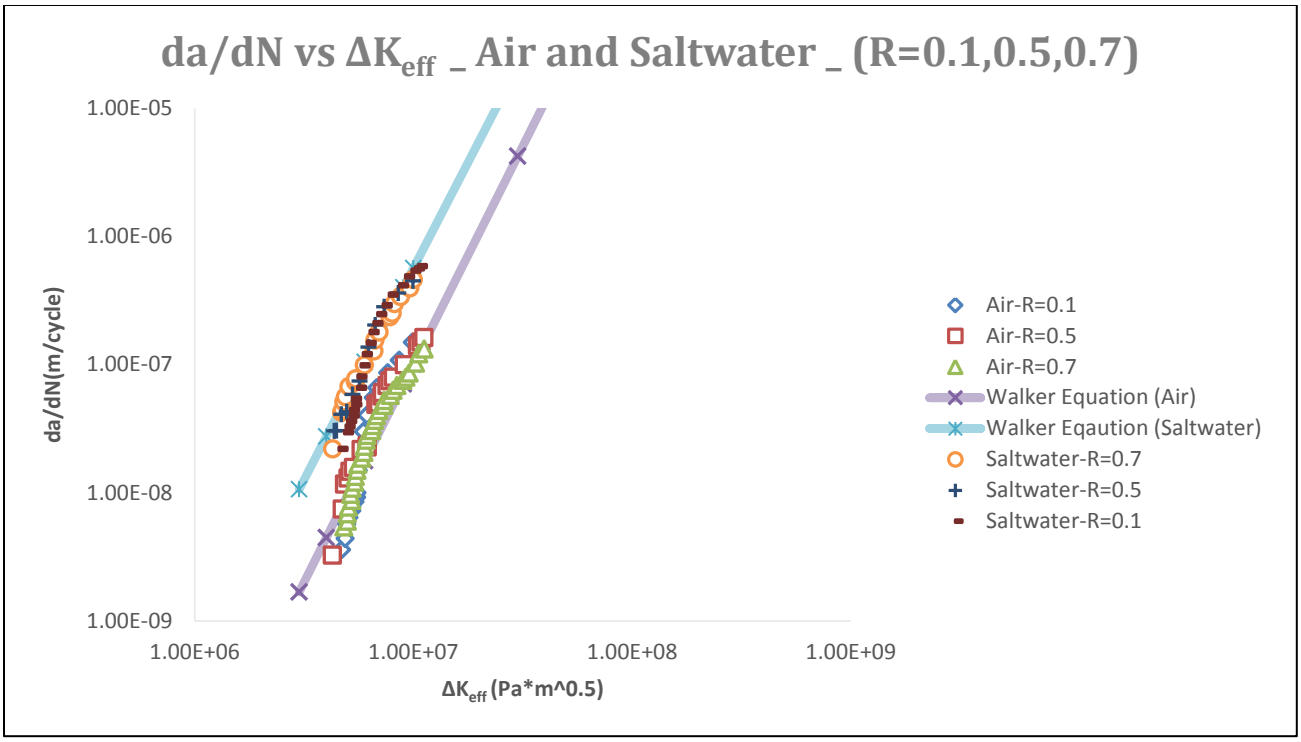

Figure 24: Combination of test data of *da/dN* versus effective *ΔK* curves for R= 0.1 ,0.5 , 0.7 in air and saltwater environments and approximation with a single relationship based on Walker equation.

The figures and the table indicates that the Walker equation collapses the fatigue crack growth rate data at stress ratio of 01, 0.5, 0.7 value onto a narrow or close band and it is effectively predicting the fatigue crack growth rate at different stress ratio when using 7075-T6 cruciform specimen under biaxial fatigue.

In order to prove that the parameters of the Walker equation that calculated for different stress ratio and showed in Table 4 are correct, regression analysis has been applied. The result is shown in Table 5 for air and saltwater environments.

Table 5: Regression Analysis for Each Experiment.

Environment	$R_{x,y}$	$\mathbf{R^2}$	**Error**
Air	0.1	0.899	0.101
Air	0.5	0.941	0.059
Air	0.7	0.934	0.066
Saltwater	0.1	0.931	0.069
Saltwater	0.5	0.963	0.037
Saltwater	0.7	0.947	0.053

From Table 5, (7.5% on average) the error of the experimental fatigue crack growth rates for 7075-T6 at stress ratio of 0.1, 0.5, 0.7 in air environment compared to those predicted by the Walker equation. similarly, (5.3% on average) the error in saltwater environment. In addition, Figure 25, Figure 26, Figure 27, Figure 28, Figure 29 and Figure 30 shows the comparison of the experimental fatigue crack growth rates for 7075-T6 at stress ratio of 0.1, 0.5, 0.7 in air and saltwater environments and those predicted by the Walker equation.

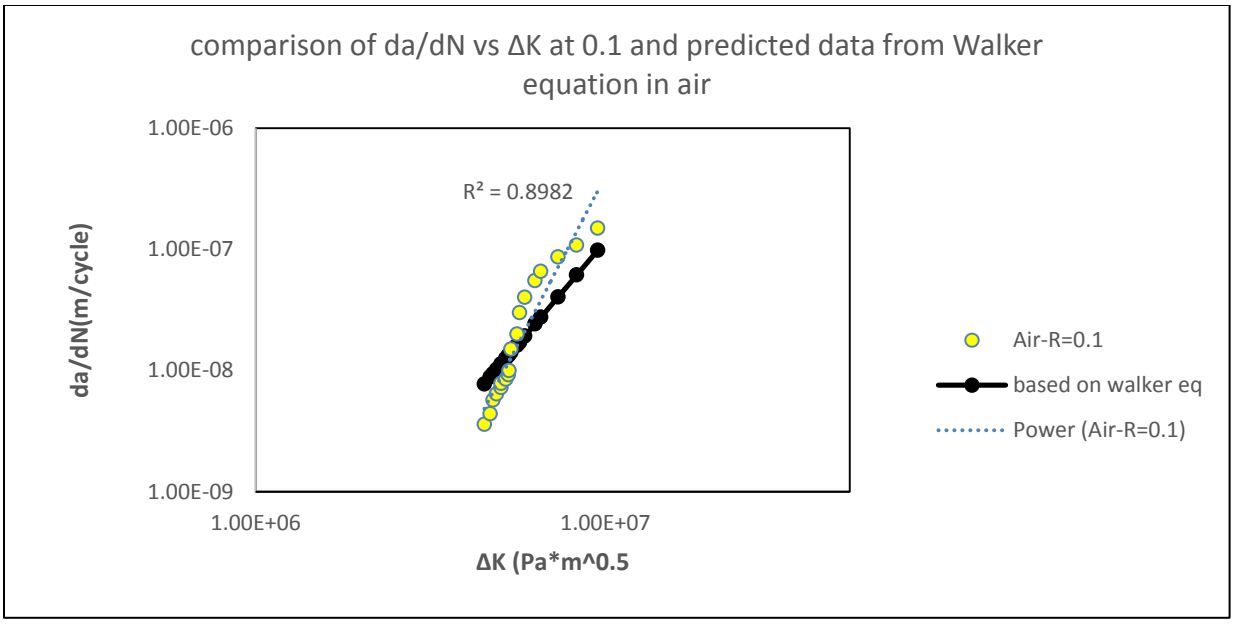

Figure 25: Comparison of the experimental fatigue crack growth rates for 7075-T6 at stress ratio of 0.1 and those predicted by the Walker equation in air environment.

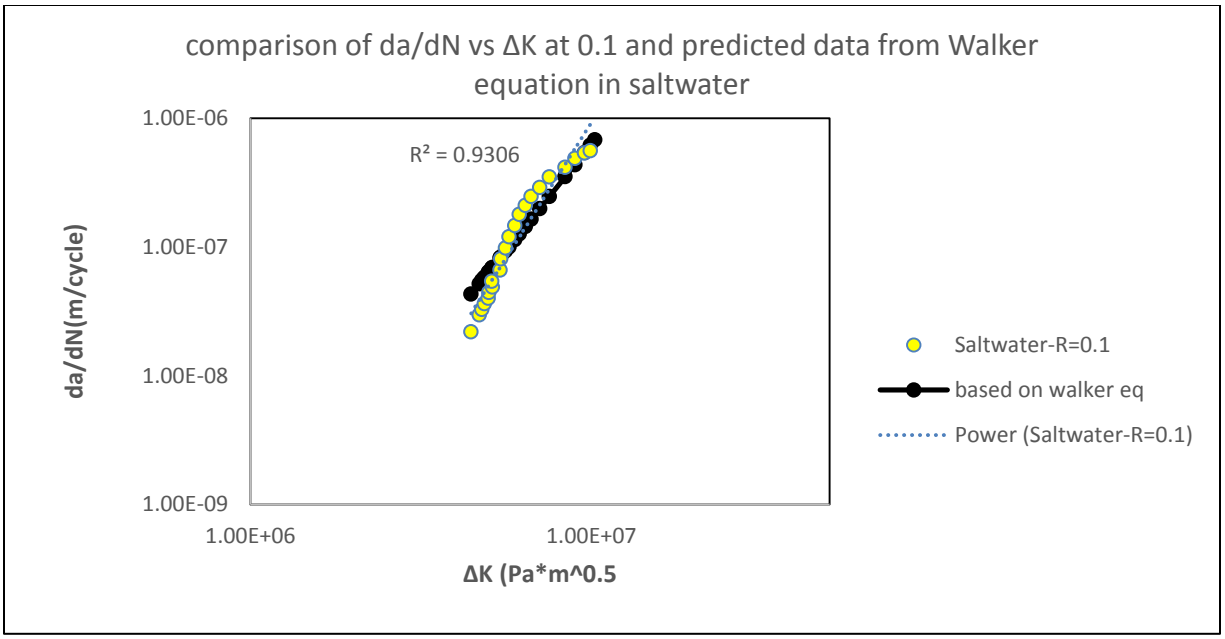

Figure 26: Comparison of the experimental fatigue crack growth rates for 7075-T6 at stress ratio of 0.1 and those predicted by the Walker equation in saltwater environment.

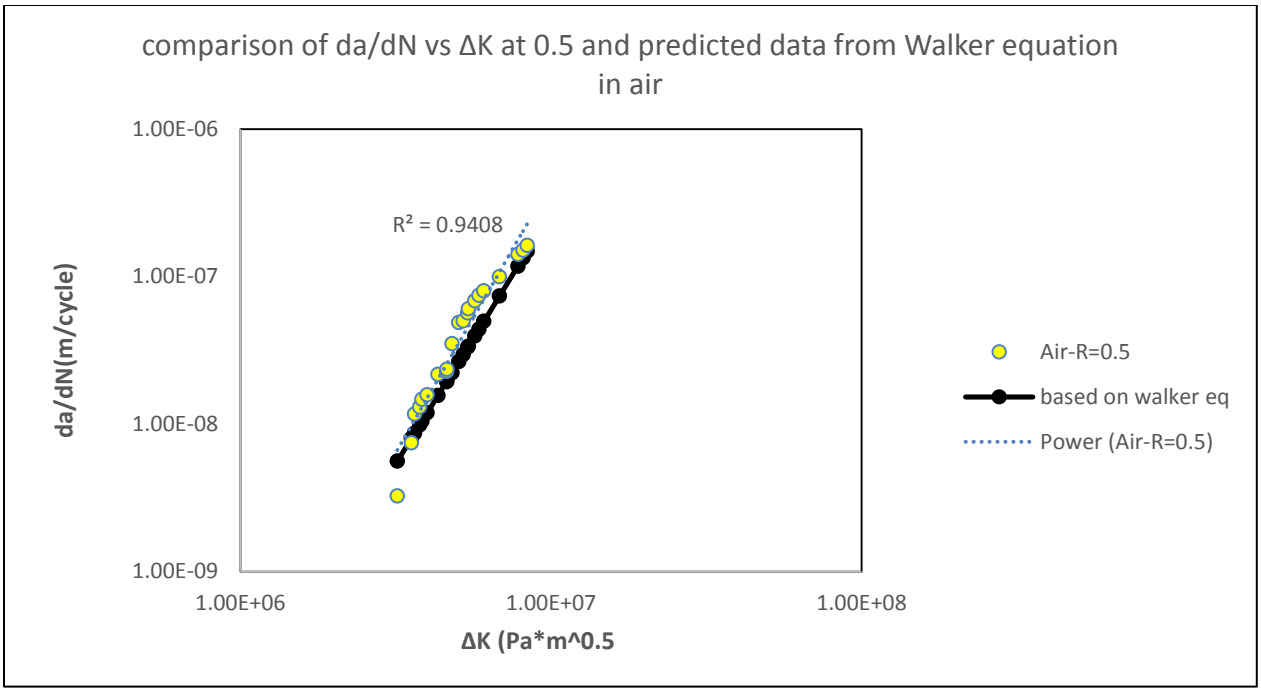

Figure 27: Comparison of the experimental fatigue crack growth rates for 7075-T6 at stress ratio of 0.5 and those predicted by the Walker equation in air environment.

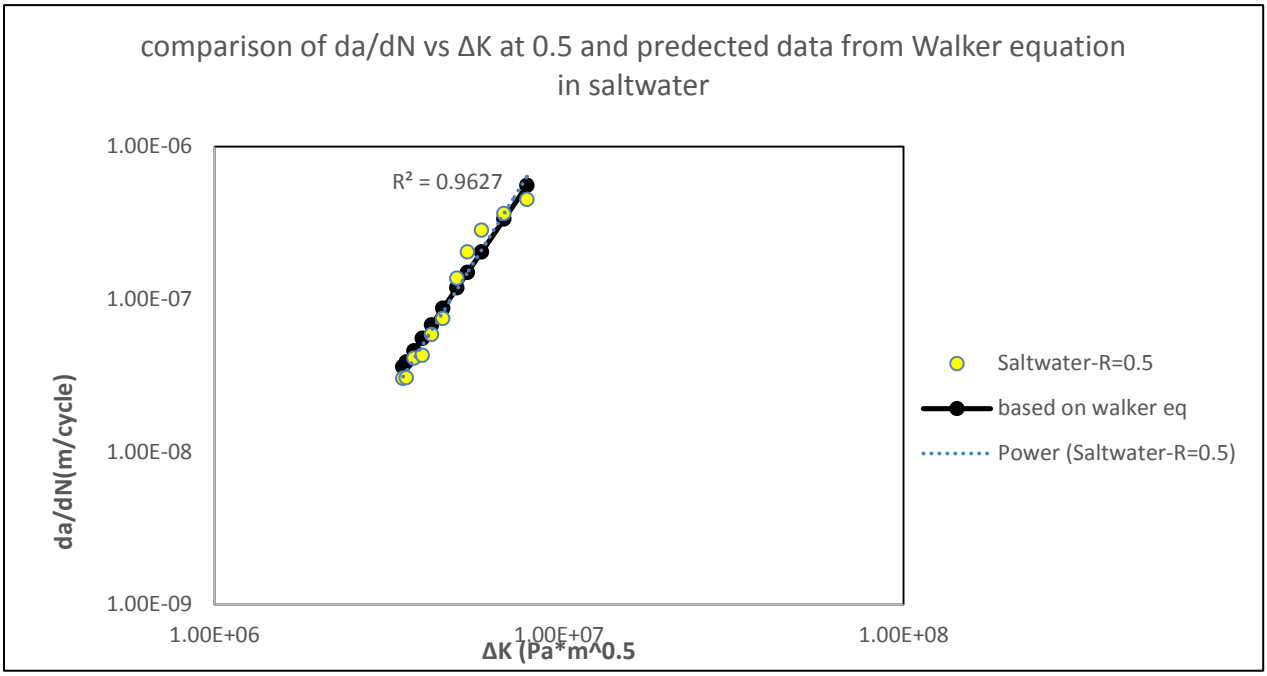

Figure 28: Comparison of the experimental fatigue crack growth rates for 7075-T6 at stress ratio of 0.5 and those predicted by the Walker equation in saltwater environment.

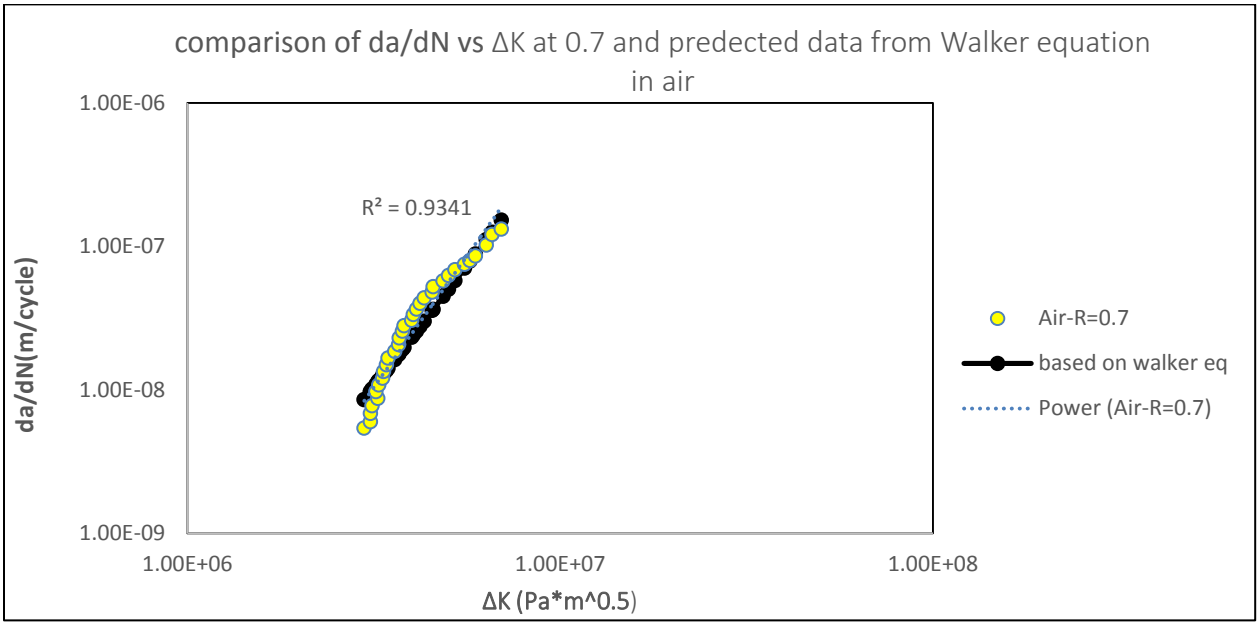

Figure 29: Comparison of the experimental fatigue crack growth rates for 7075-T6 at stress ratio of 0.7 and those predicted by the Walker equation in air environment.

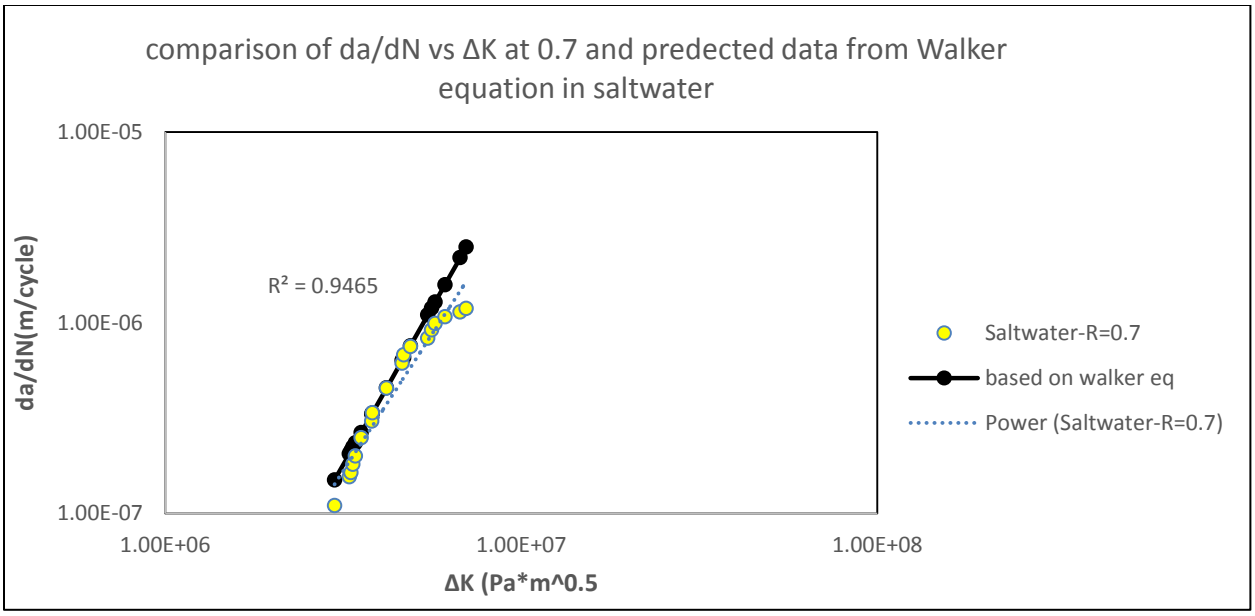

Figure 30: Comparison of the experimental fatigue crack growth rates for 7075-T6 at stress ratio of 0.7 and those predicted by the Walker equation in saltwater environment.

VI. Conclusions and Recommendations

6.1 Conclusions

The present research studied the fatigue crack growth behavior in cruciform specimen made from 7075-T6 aluminum alloy. The crack growth was inspected under in-plane biaxial loading in both air and saltwater (3.5% NaCl) environments for wide range of R-ratio: R= 0.1, 0.5 and 0.7. The biaxility ratio λ=1 was fixed throughout the test. The experiments were conducted and data was collected. The results of this study show the effect of stress ratio on the fatigue crack growth rate in air and saltwater environments Fracture mechanics was used in this research to generate more accurate definition of

Walker equation parameters. It leads to more accurate prediction of fatigue crack growth rate at different stress ratio. The following conclusion can be drawn from this research:

1. The crack paths for all cases in laboratory air and saltwater environments was collinear with the notch. The crack grows in a straight line under 45° to the directions of the applied forces. There is no effect of the stress ratio on crack path direction.
2. The stress ratio increase leads to increase in fatigue crack growth rate in both laboratory air and saltwater environments.
3. The fatigue crack is grown 50 % faster in saltwater (3.5% NaCl) environment comparatively with air environment.
4. Parameters of Walker equation calculated using the received experimental data were shown in the table

Environment	m	γ	C_0 **(m/cycle)**
Air	3.4	0.6	16×10^{-32}
Saltwater	3.3	0.7	4.5×10^{-30}

5. The effective fatigue crack growth rate predicted by Walker equation is very close to effective fatigue crack growth rates generated by the test in air and saltwater environment.

6. The error of the experimental fatigue crack growth rates for AA 7075-T6 at stress ratio of 0.1, 0.5, 0.7 compared to those predicted by the Walker equation is 7.5% in air environment and 5.3% in saltwater environment.
7. The research indicates the effective predicting for the fatigue crack growth rate at different stress ratio when using cruciform specimen made from 7075-T6 aluminum alloy under biaxial loading.

6.2 Recommendations

There are wide range of test variables can be changed to provide useful information about the behavior of fatigue crack growth rate initiated from circular hole for 7075-T6 aluminum alloy under biaxial loading. Another research might focus on studying the behavior of fatigue crack growth rate from circular hole of 7075-T6 aluminum alloy for negative values of stress ratio.

Further researches in fatigue crack growth form circular hole could be conducted on different materials under biaxial loading.

Appendix A: Finite Element Approach (FEA)

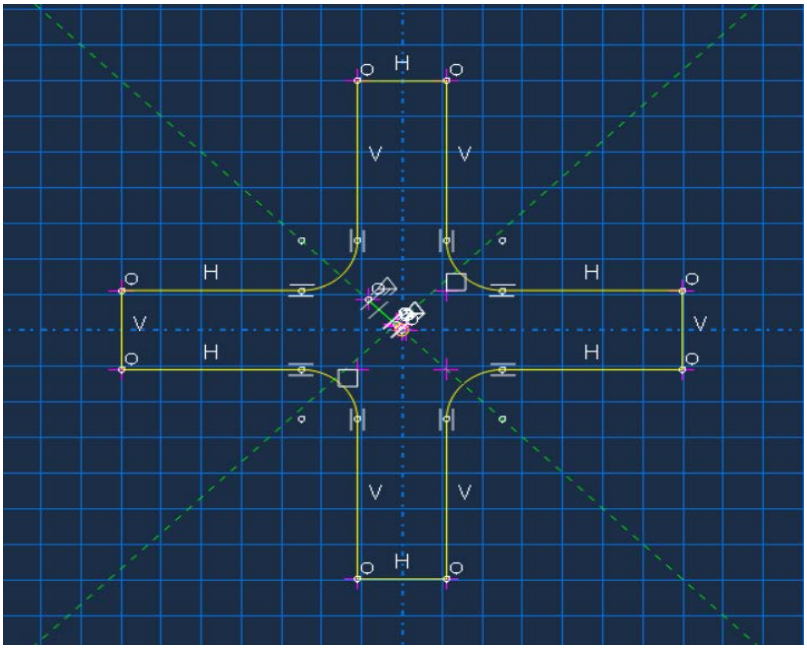

Figure 31: Sketch of the specimen in Abaqus.

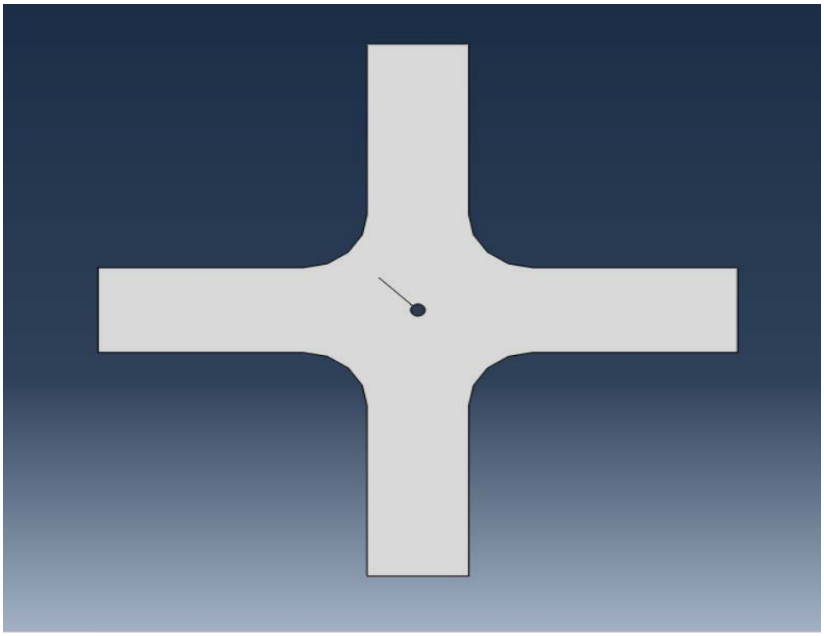

Figure 32: The whole part of the specimen in Abaqus program including the crack.

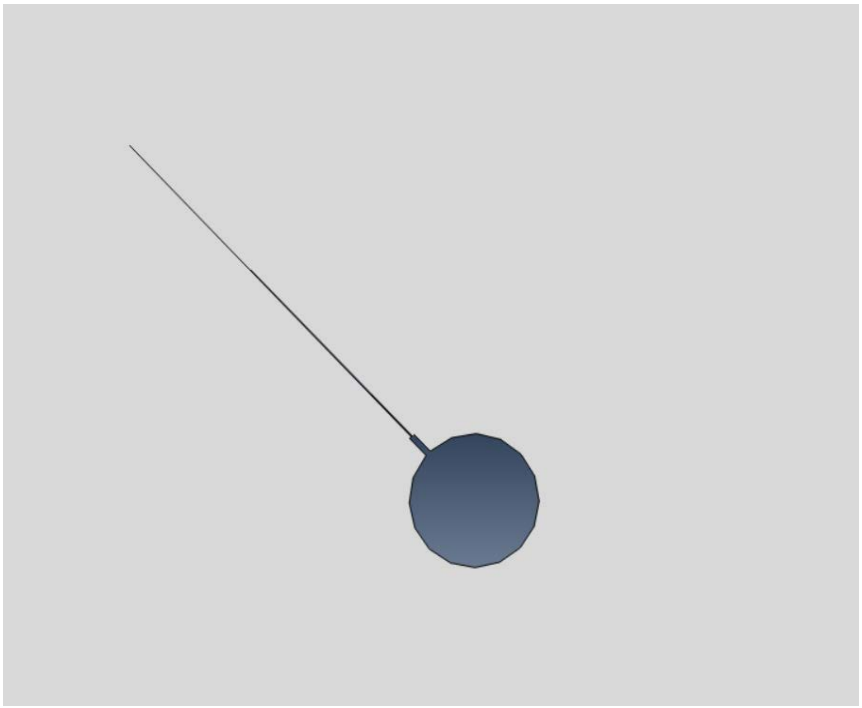

Figure 33: A closer picture to the hole, notch, pre-crack and the crack in one of the specimens in Abaqus program.

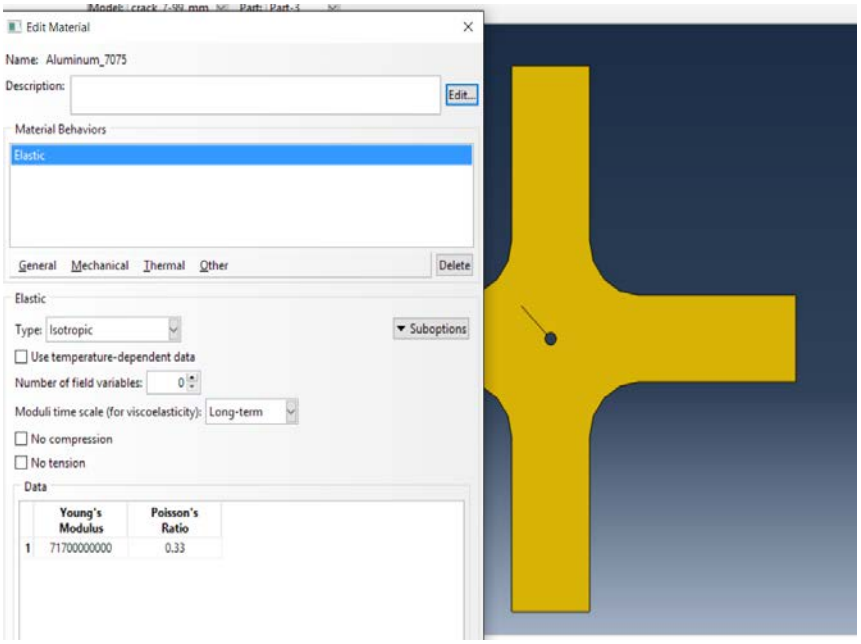

Figure 34: Assigning the material type to the specimen, 7075-T6 aluminum alloy.

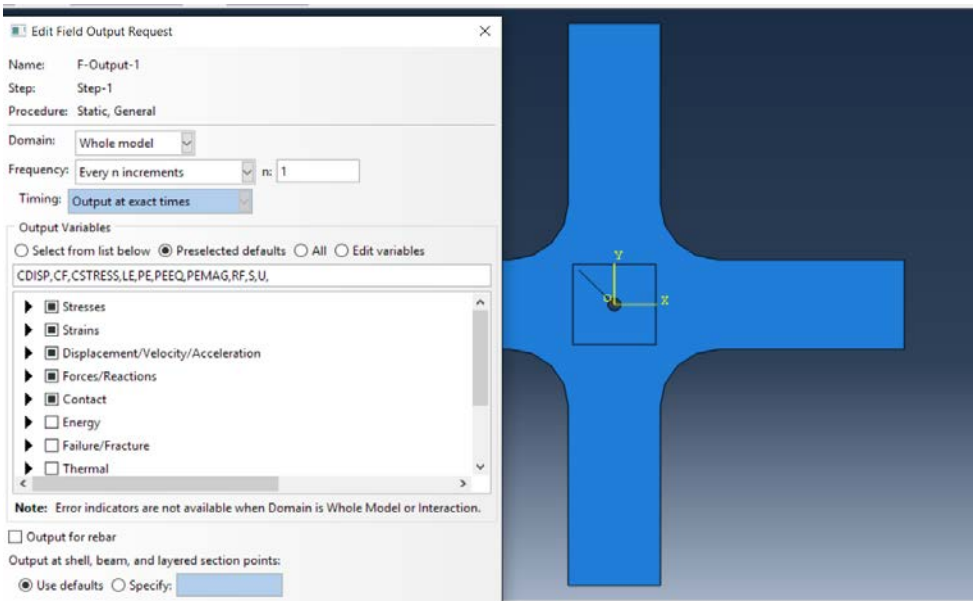

Figure 35 Specifying the needed calculated output, ΔKs and cracks' directions are our concern.

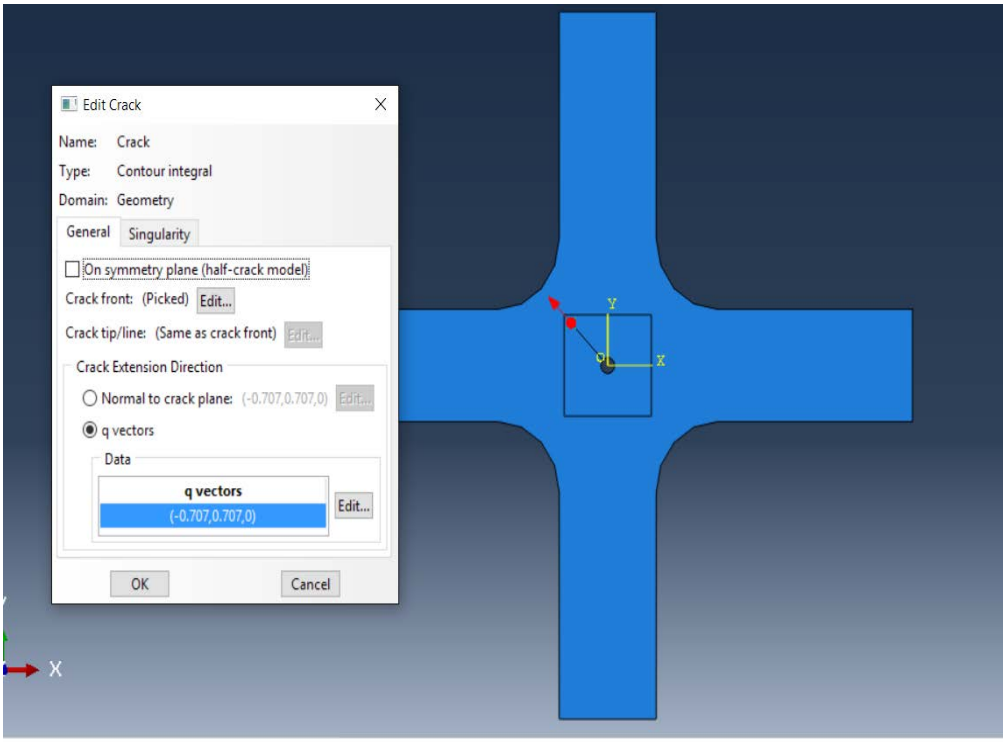

Figure 36: Specifying the location and the direction of crack-tip.

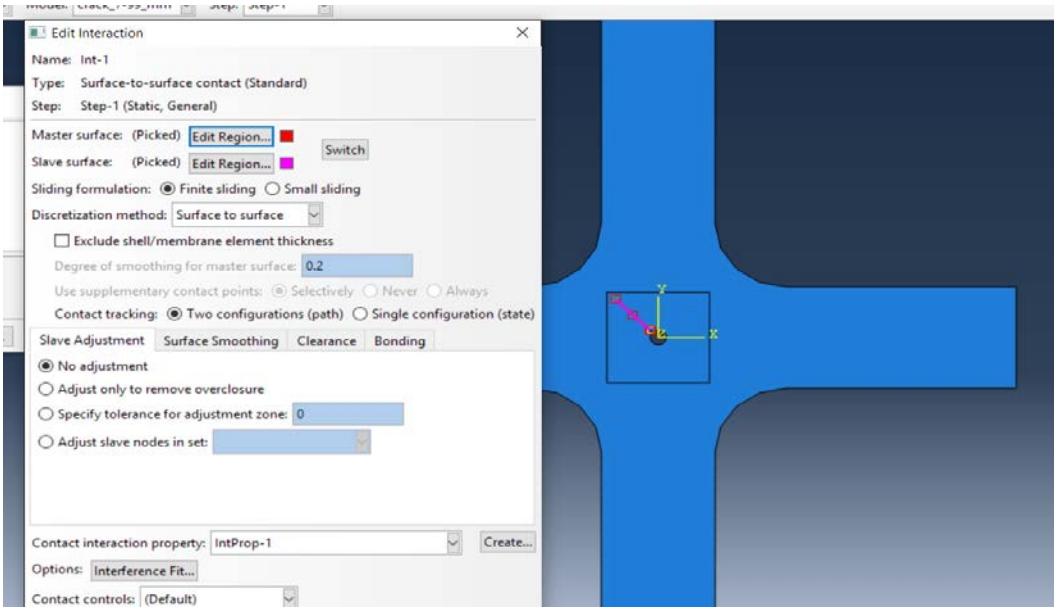

Figure 37 Selecting the masters' and the slaves' edges and setting the boundary conditions to the crack (No Friction between the Adjacent Surfaces of a Certain Crack).

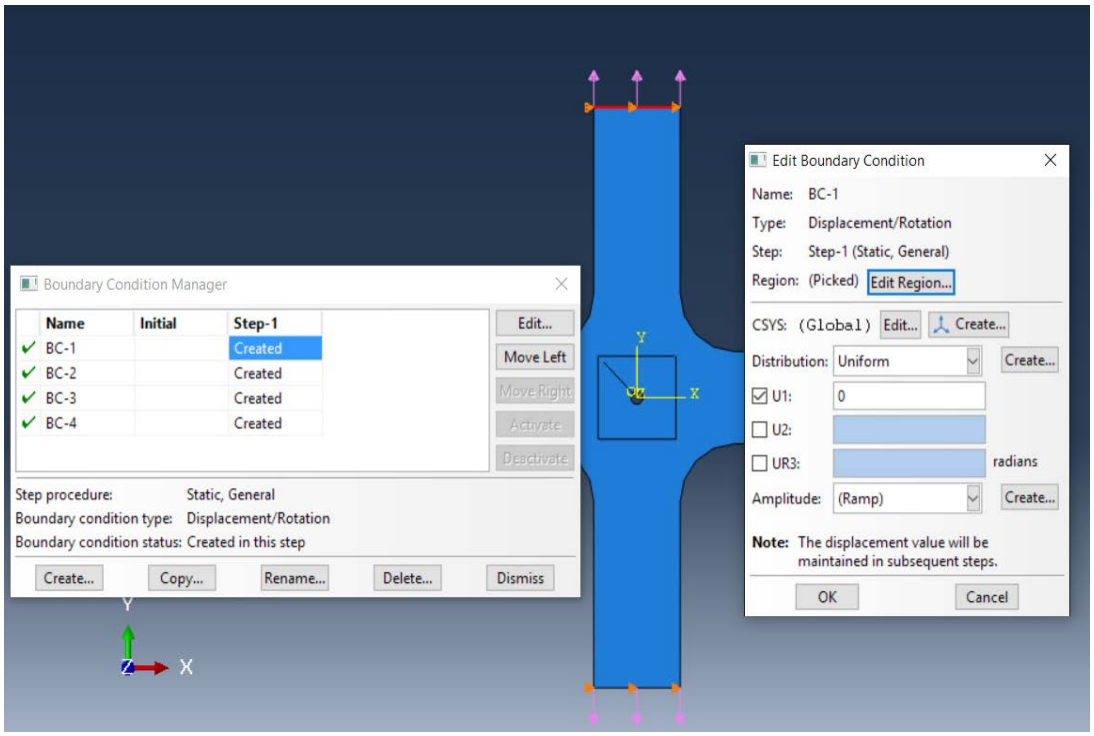

Figure 38 Specifying the boundary condition to the vertical end arms of the specimen.

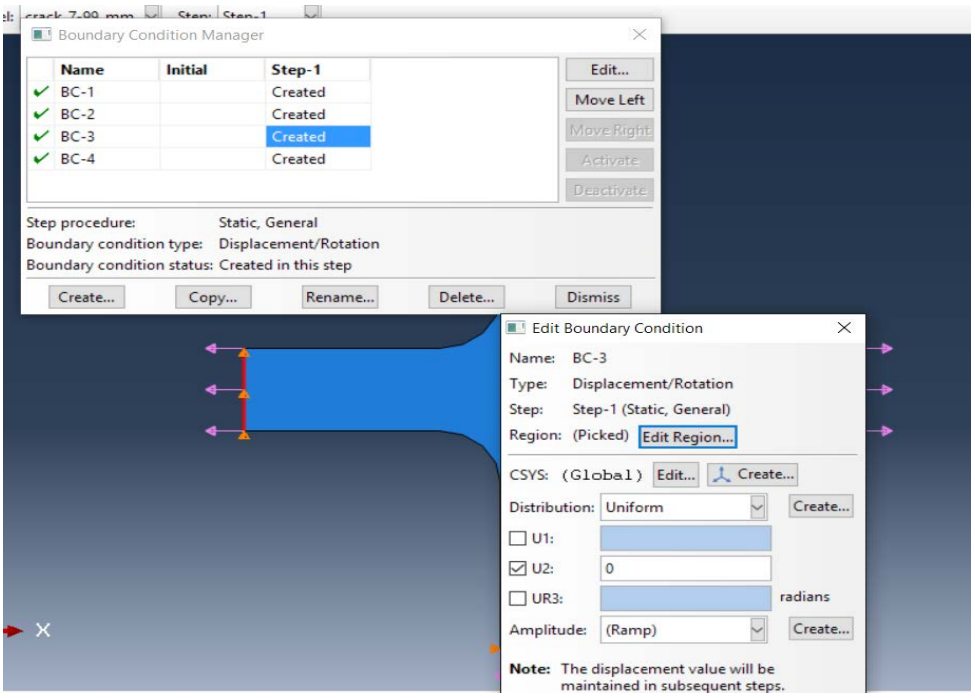

Figure 39: Specifying the boundary condition to the horizontal end arms of the specimen.

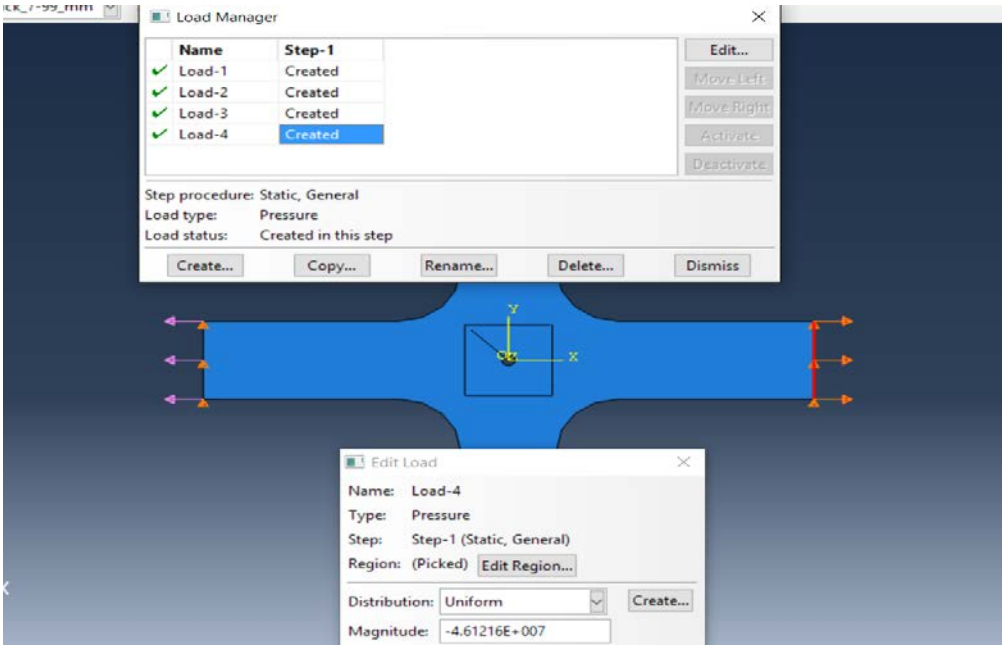

Figure 40: Specifying the loads to the horizontal arm end of the specimen.

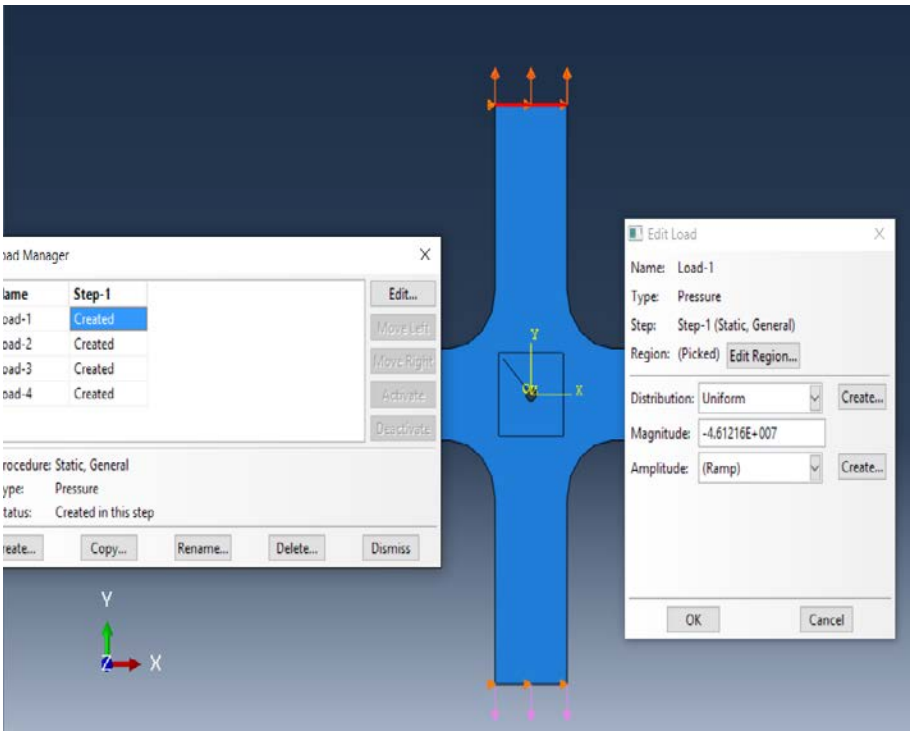

Figure 41: Specifying the dynamic loads to the vertical arm end of the specimen.

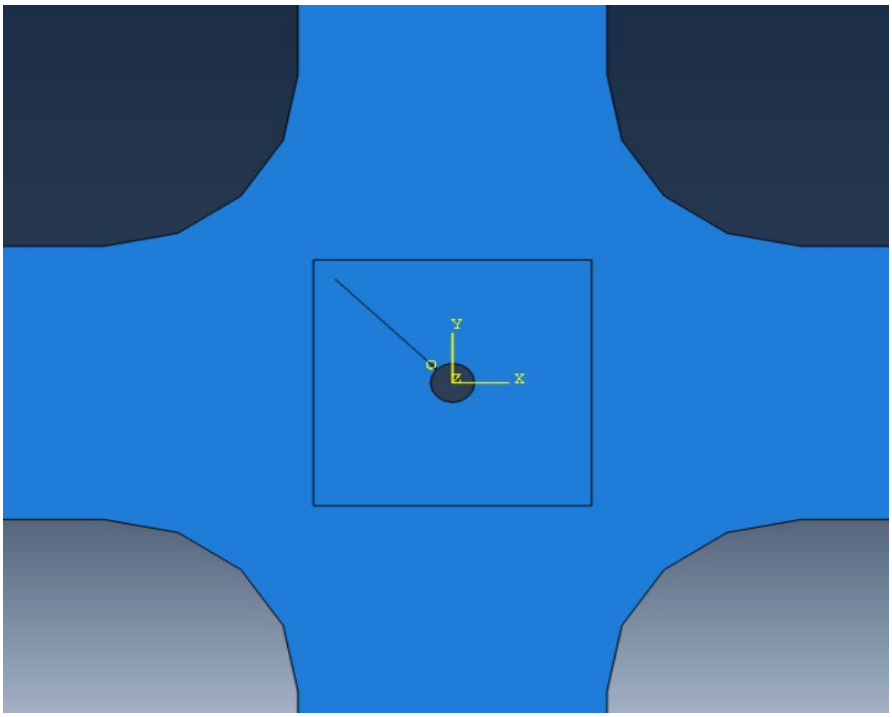

Figure 42 Creating a partition for high density mesh in order to get more accurate results.

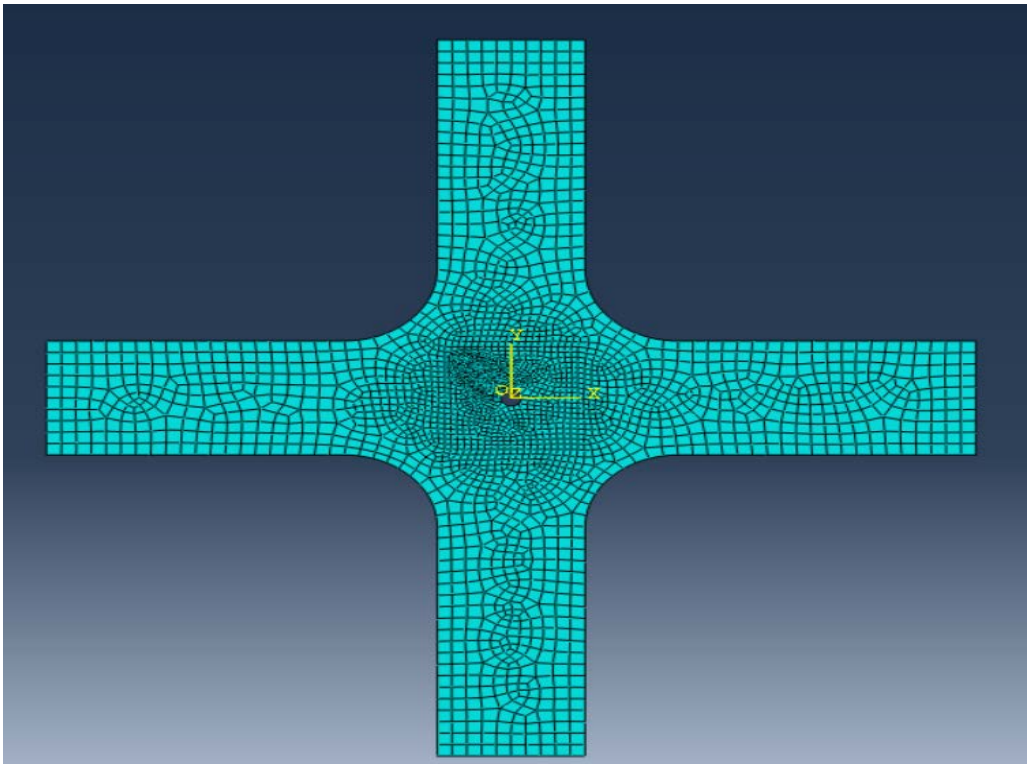

Figure 43: Meshing the specimen including the area with high mesh density.

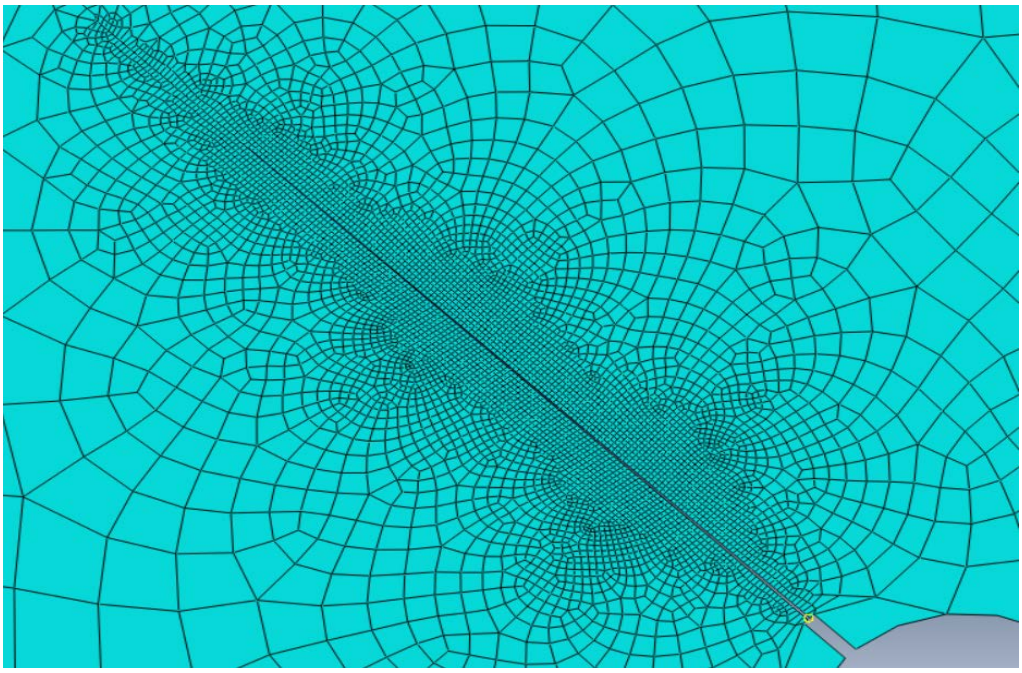

Figure 44: A closer look of the high mesh density area.

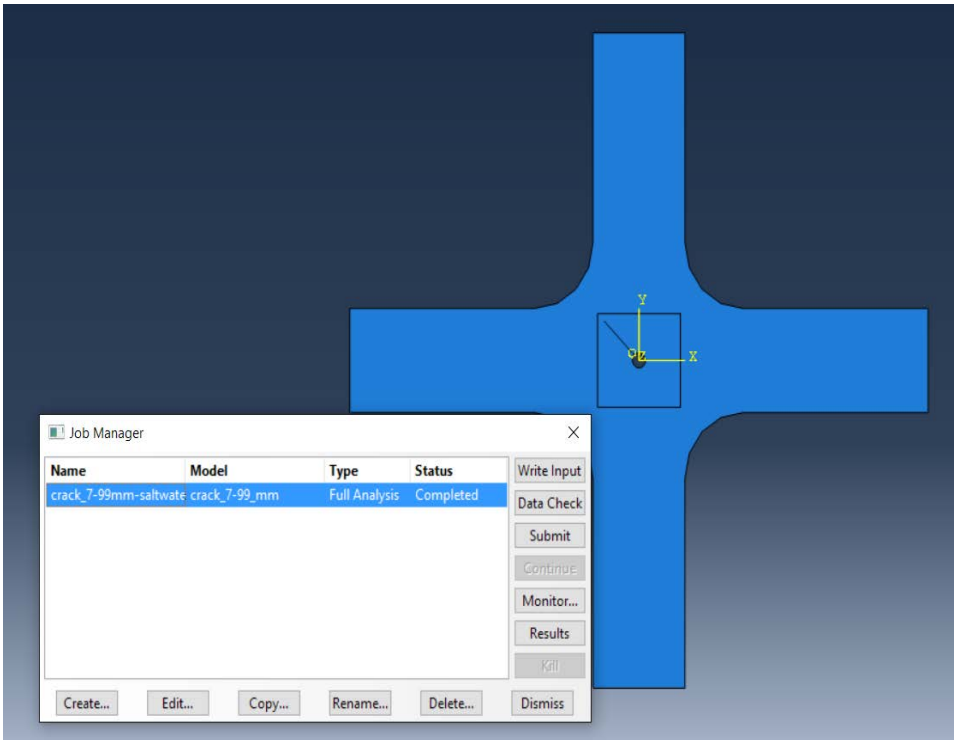

Figure 45: Creating a job order to get results.

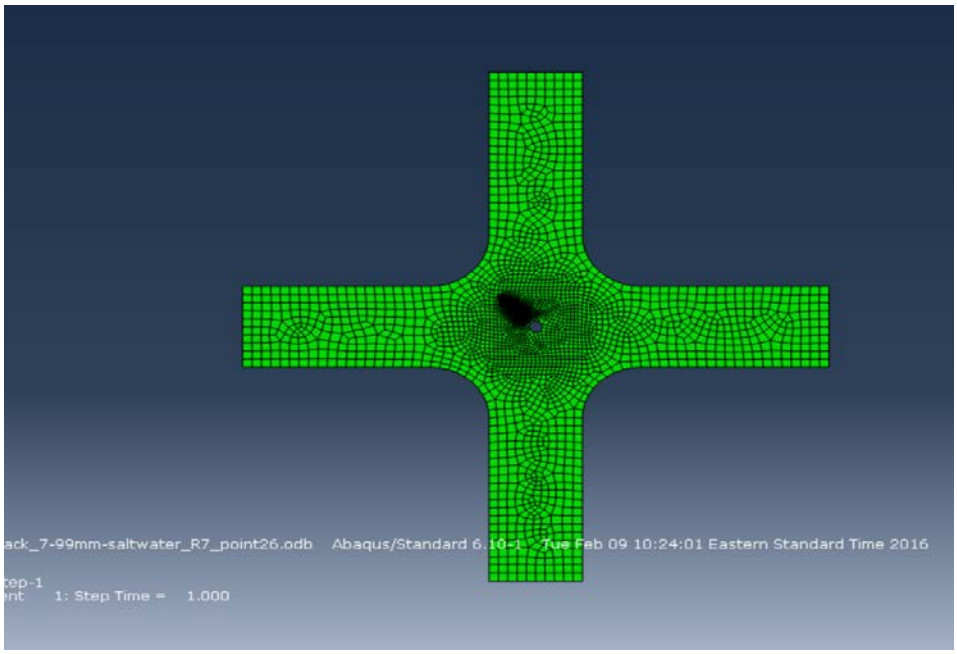

Figure 46: The specimen after submitting the job order.

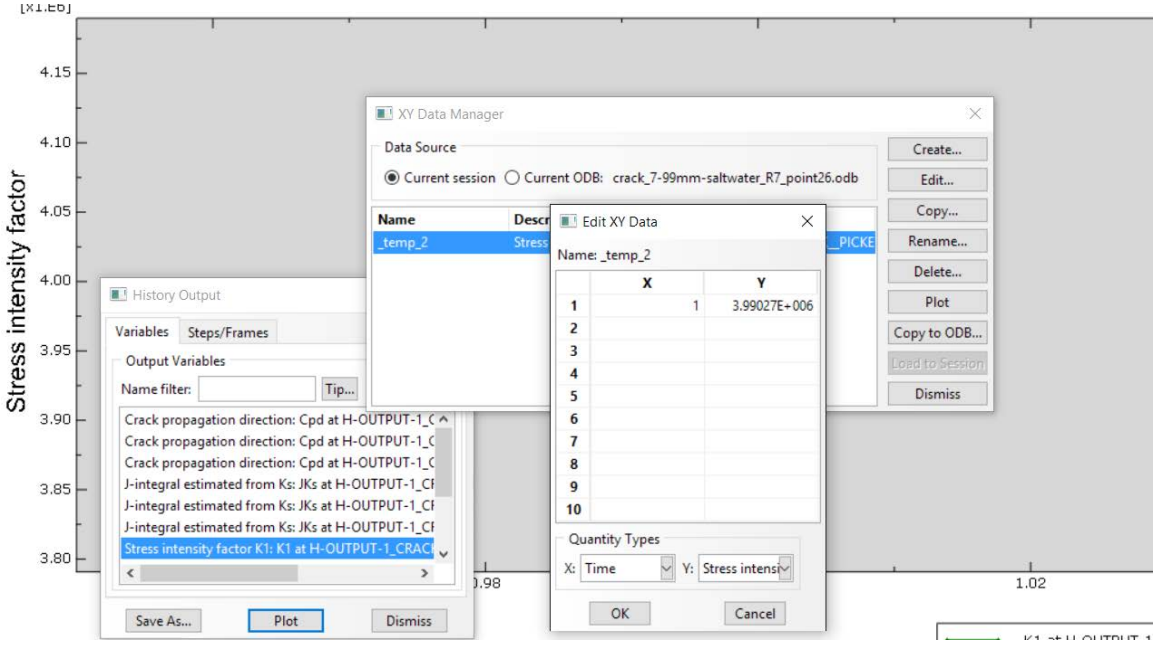

Figure 47: The final step of each point's result.

Appendix B: Pictures of Cracks at Different Stress Ratios, Conditions and Environments

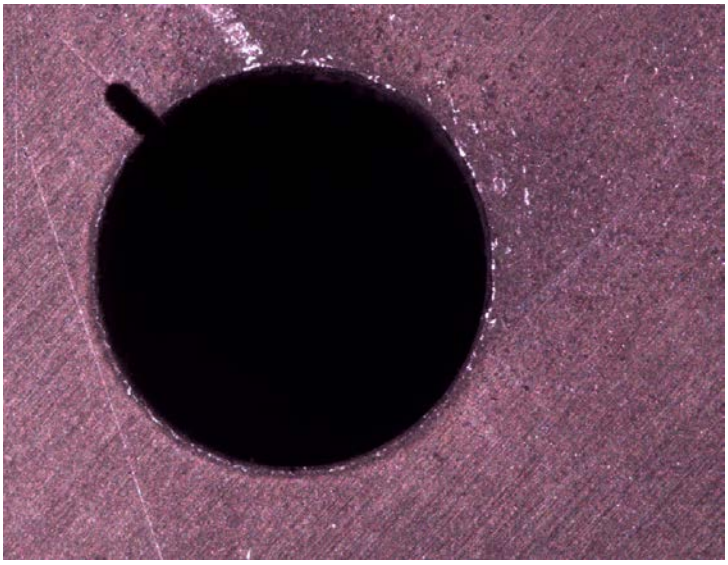

Figure 48: Specimen with 1mm length pre-crack at the fatigued at R=0.1 in air environment.

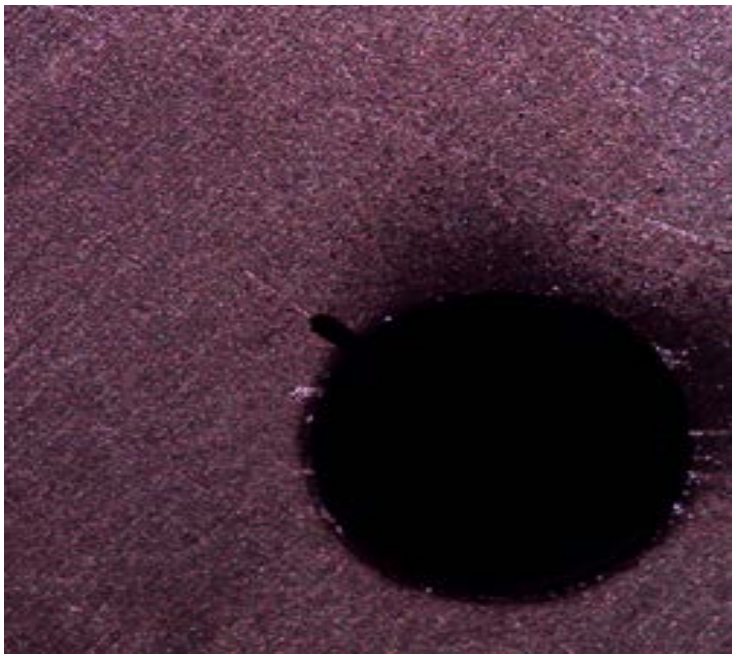

Figure 49: 1.46 mm crack length after 105,000 fatigue cycles at R=0.1 in air environment.

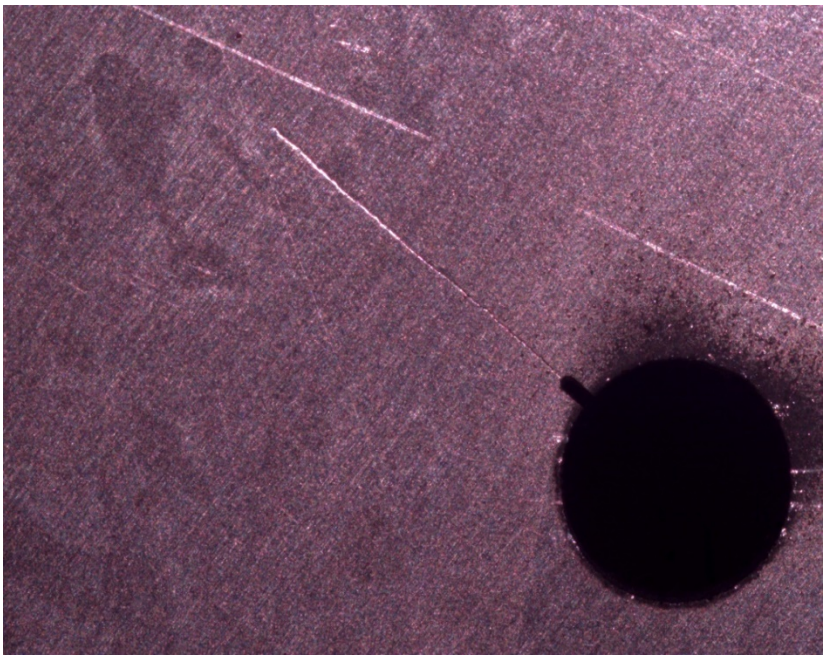

Figure 50: 13.33 mm crack length after 455,000 fatigue cycles at R=0.1 in air environment.

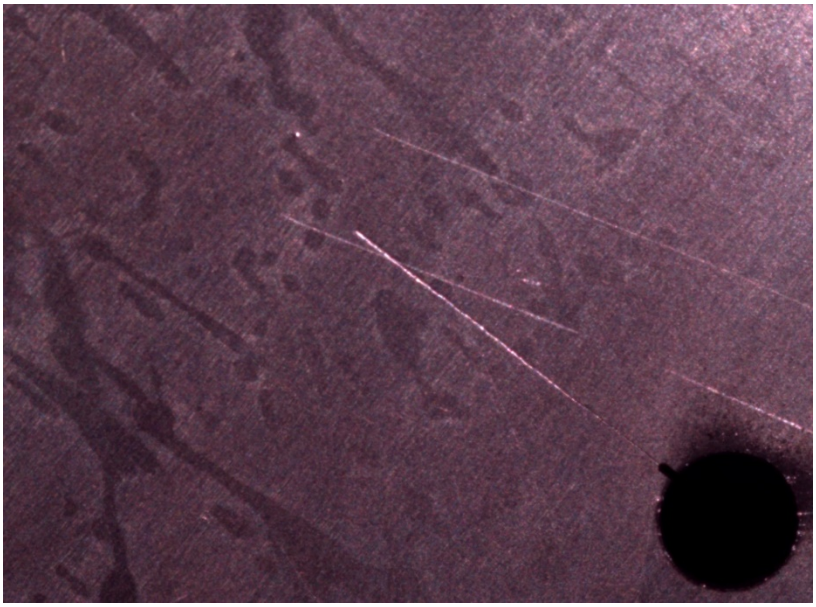

Figure 51: Crack before failure in air environment.

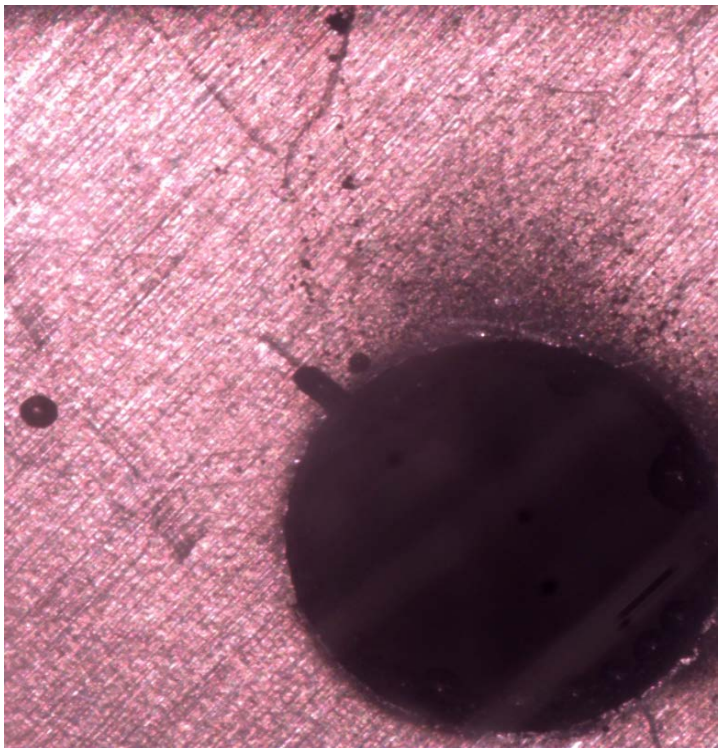

Figure 52: 1 mm length pre-crack of 1 mm length in saltwater environment.

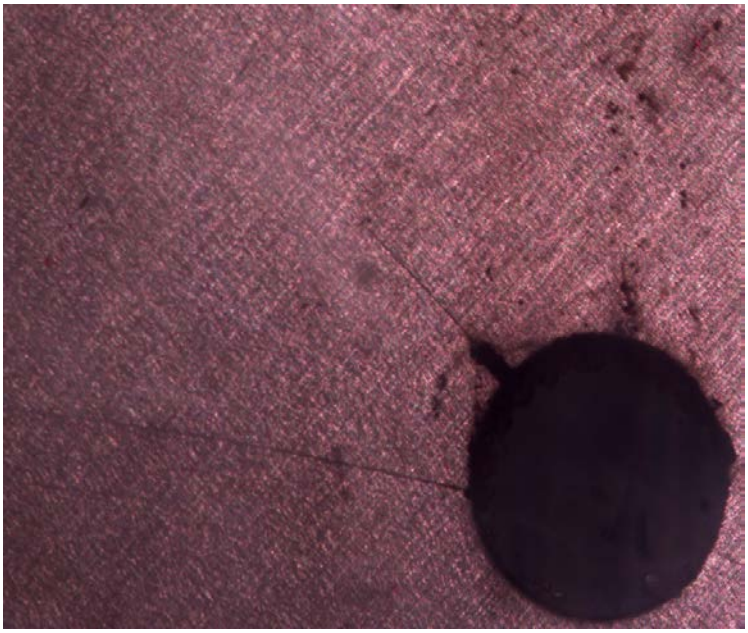

Figure 53: Crack of 3.58 mm length after applied 75,000 fatigue cycles in saltwater environment at stress ratio of 0.1.

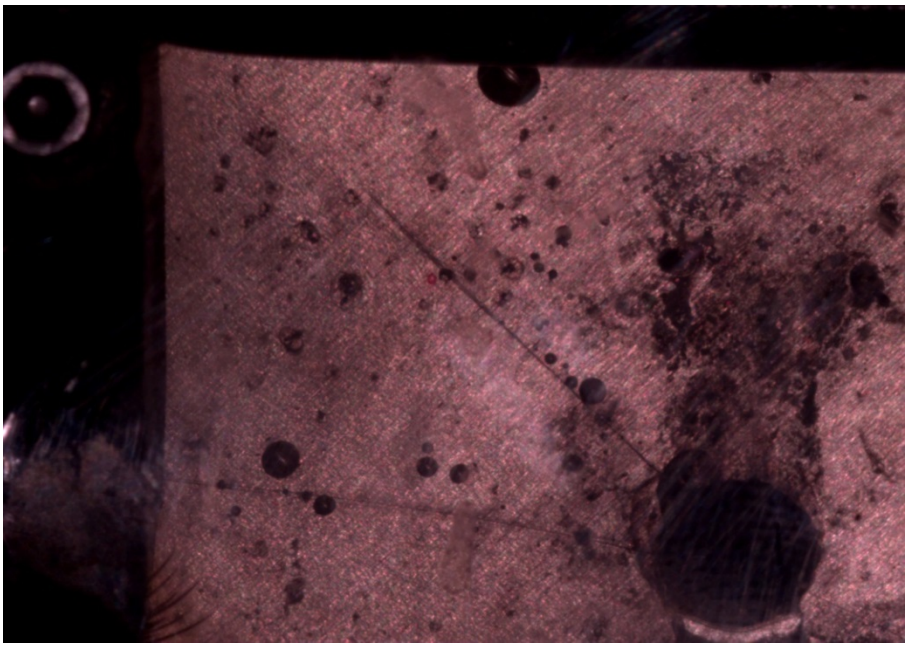

Figure 54: Crack before failure while running R=0.1 experiment in saltwater environment.

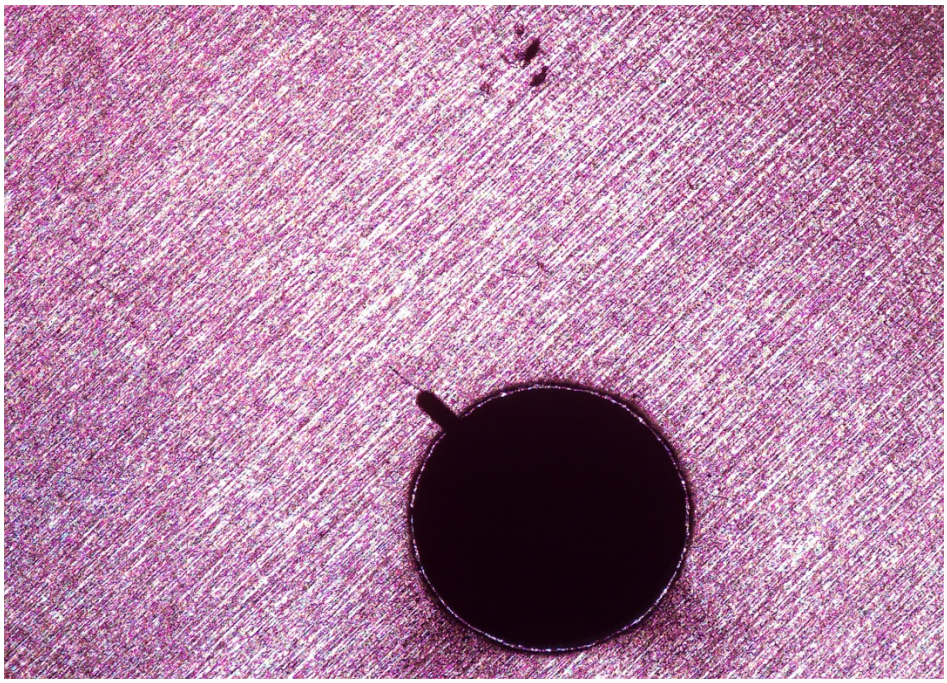

Figure 55: Specimen of 1 mm length pre-crack at the beginning of R=0.7 experiment in air environment.

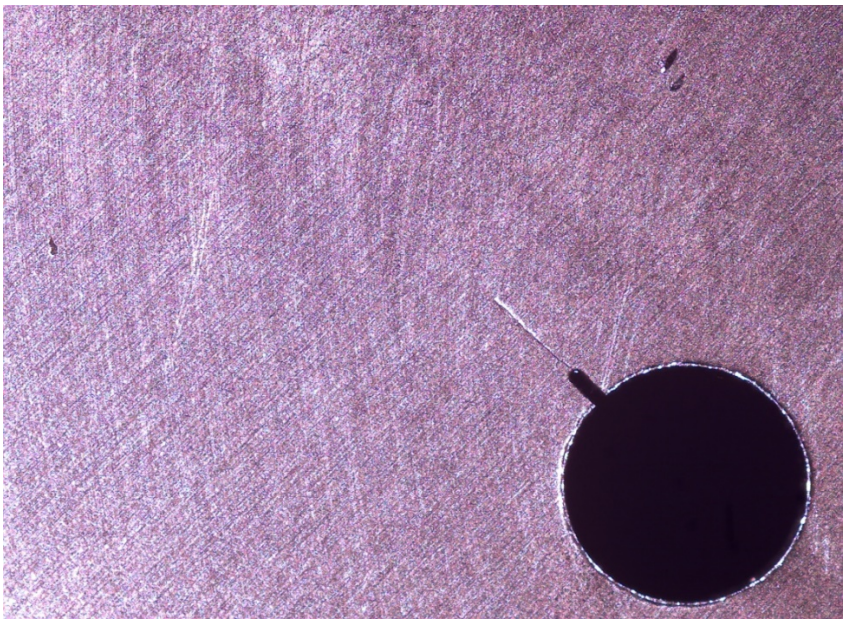

Figure 56: 2.2 mm length crack after applied188,000 fatigue cycles in air environment at stress ratio of 0.7 .

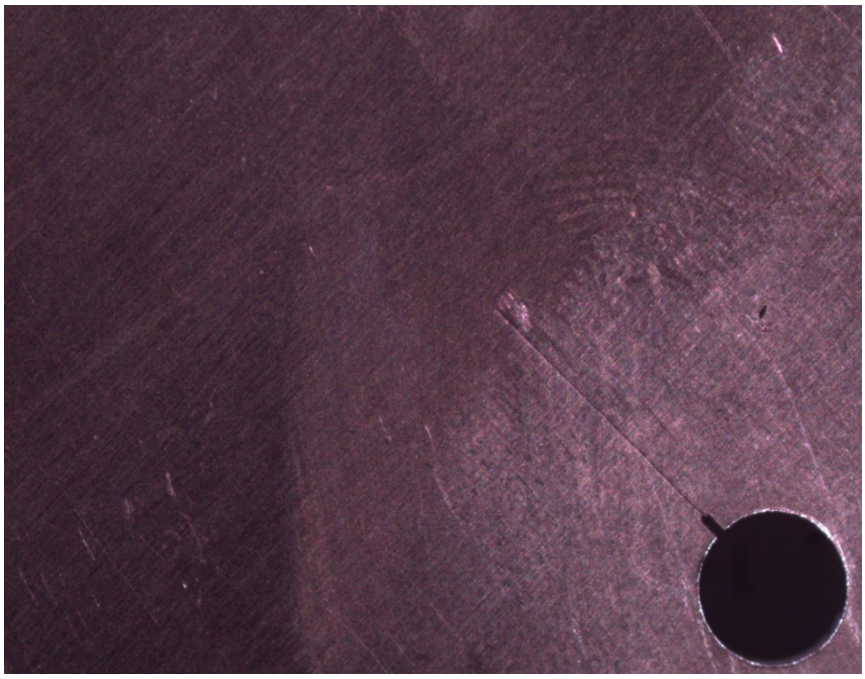

Figure 57: Crack before failure while running R=0.7 experiment in air environment.

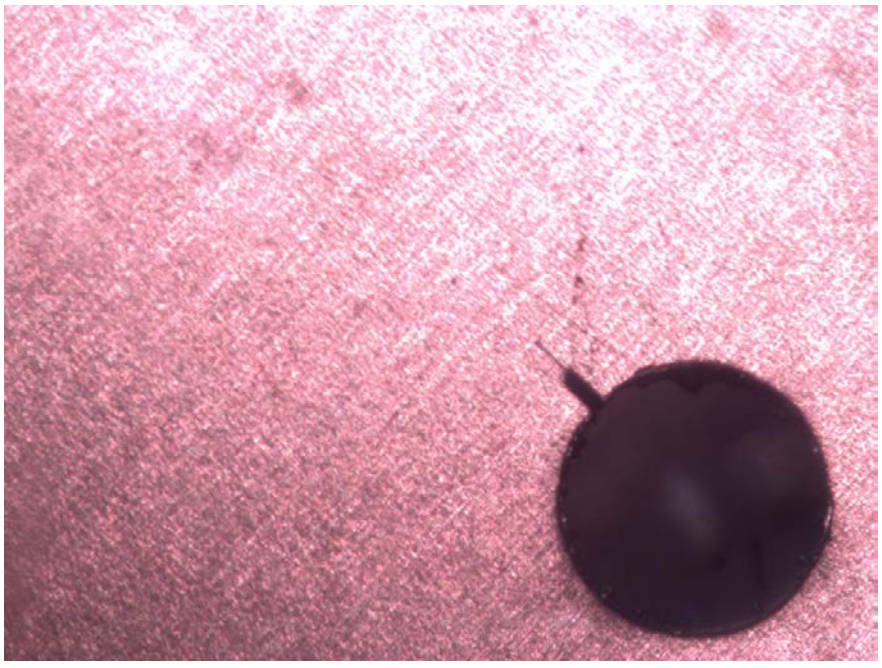

Figure 58: Specimen of 1 mm length pre-crack at the beginning of R=0.7 experiment in saltwater environment.

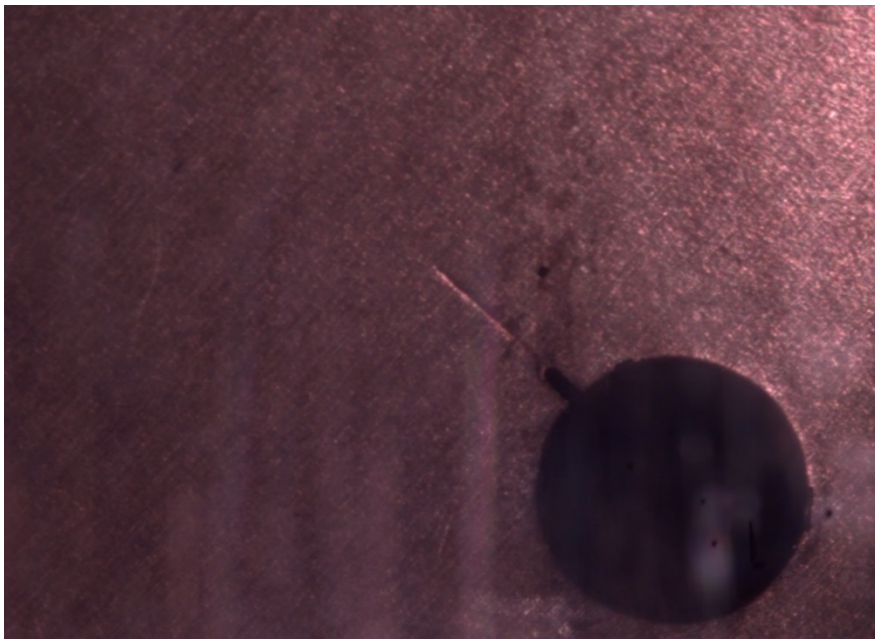

Figure 59: 3.44 mm length crack after applied 92,000 fatigue cycles in saltwater environment at stress ratio of 0.7.

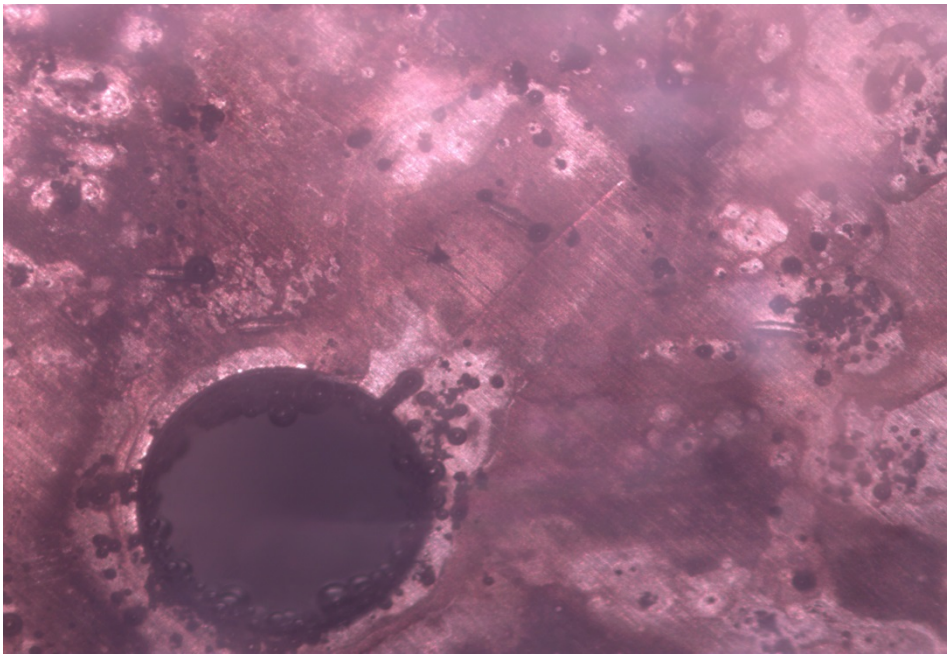

Figure 60: 6.04 mm length crack after applied 142,000 fatigue cycles in saltwater environment at stress ratio of 0.7.

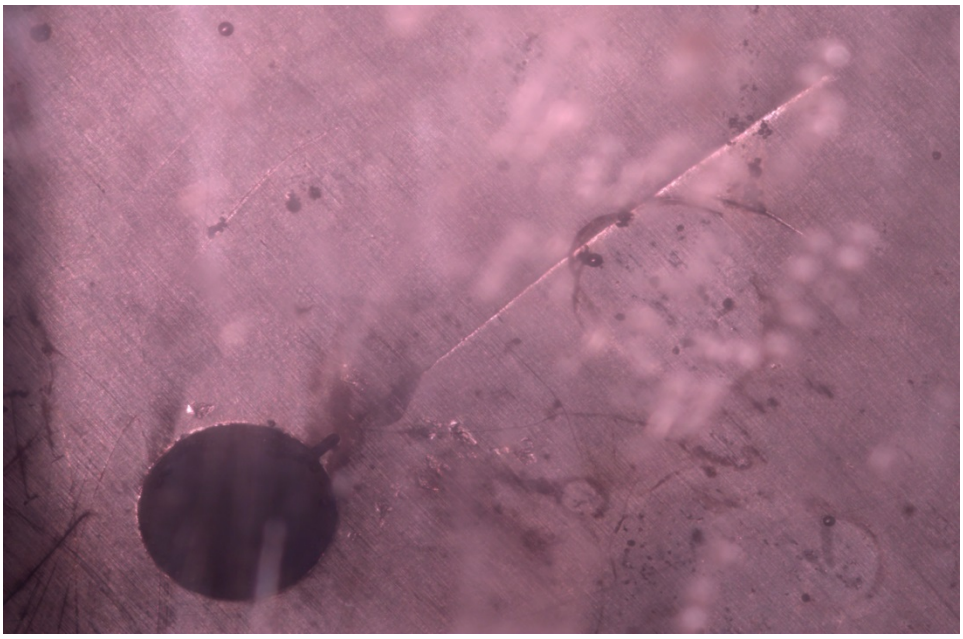

Figure 61: Crack before failure while running R=0.7 experiment in saltwater environment.

Appendix C: Crack Length versus Number of Cycles Curves at Different Stress Ratios in Air and Saltwater Environments

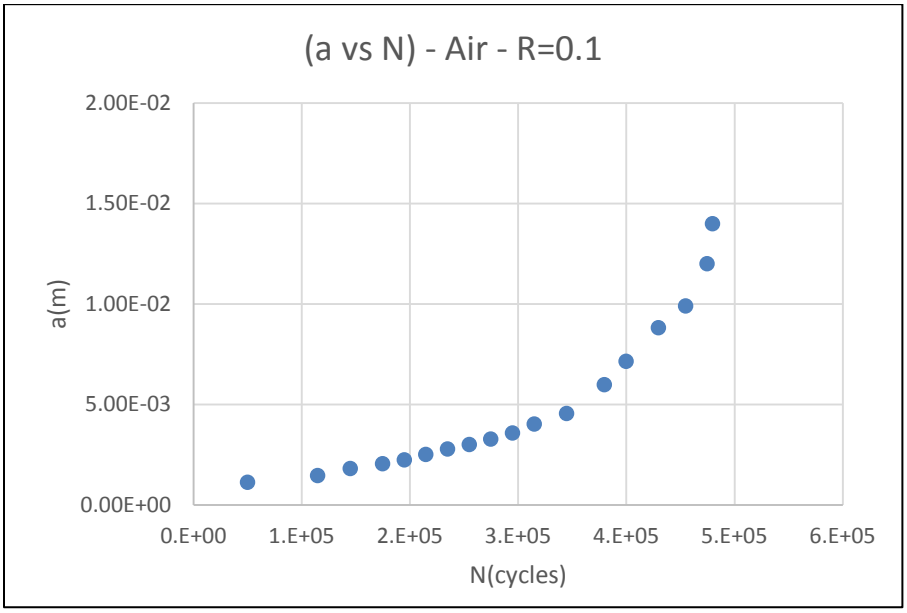

Figure 62: Crack length versus number of cycles for R=0.1 in air environment.

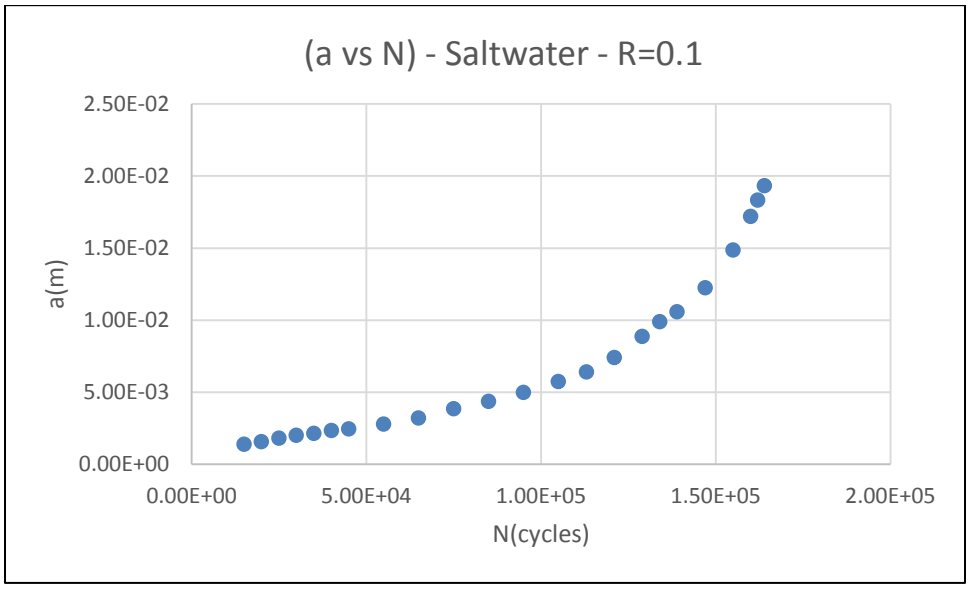

Figure 63: Crack length versus the number of cycles curve for R=0.1 in saltwater environment.

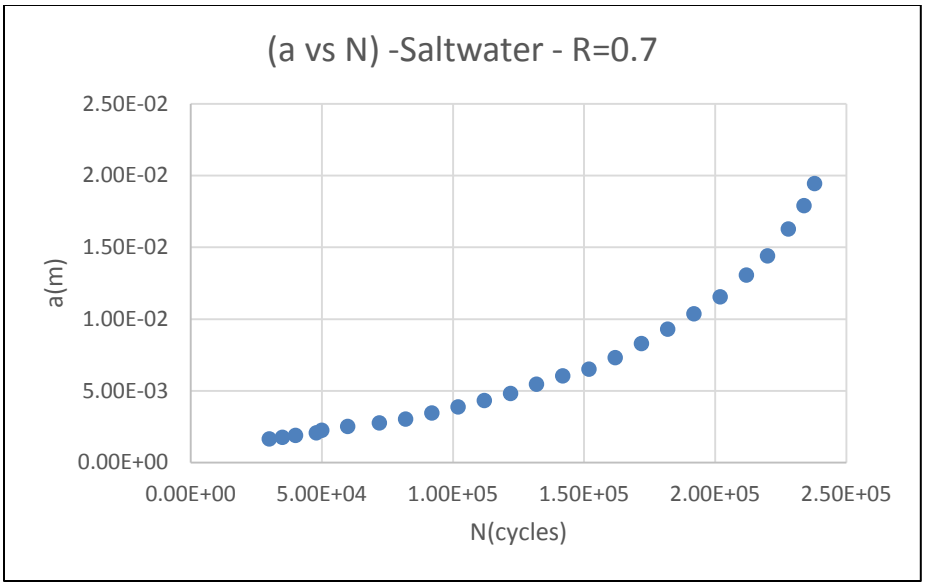

Figure 64: Crack length versus number of cycles for R=0.7 in saltwater environment.

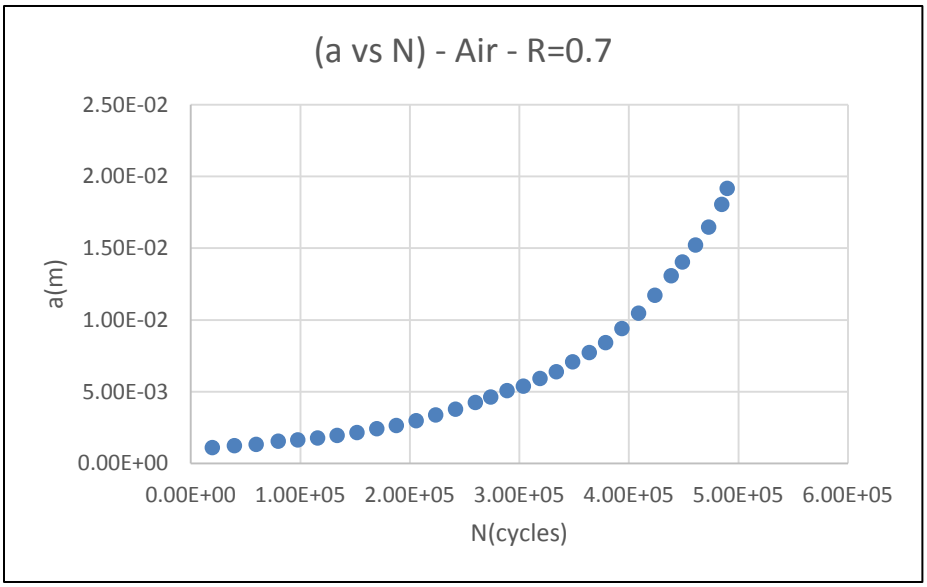

Figure 65: Crack length versus number of cycles for R=0.7 in air environment.

Bibliography

[1] 7000 Series Aluminum Alloy, Aerospace Specification Metals (ASM), http://asm.matweb.com/search/SpecificMaterial.asp?bassnum=MA7075T6. (Accessed November 2014).

[2] AHLUWALIA, HIRA. "Combating Plate Corrosion." THE FABRICATOR, 2003.

[3] Alcoa 7075 data sheet (PDF). (Accessed August 2nd, 2014).

[4] Anderson, P.R.G., and G.G. Garrett. "Fatigue Crack Growth Rate Variations in Biaxial Stress Fields." International Journal of Fracture, 16:111–116, 1980.

[5] Anderson, T.L., Fracture Mechanics: Fundamentals and Applications, 3rd edition, Taylor and Francis, 2005.

[6] Berezhnitski, L.T., and R.S. Gromyak. "Evaluation of Limiting State of Matrix in Vicinity of Sharp-Edge Rigid Inclusion." Material Science, Volume 13, Number 2, 1977.

[7] Borisenko, Tarapov, Vector and Tensor Analysis with Applications, 1968.

[8] Castro P.M.S.T., P.F.P. Matos, G.P. Moreira, and L.F.M. Silva. "An Overview on Fatigue Analysis of Aeronautical Structural Details: Open Hole, Single Rivet Lap-Joint, and Lap-Joint Panel." Materials Science and Engineering: A, 468-470:144–157, 2007.

[9] Davis, JR. "Corrosion of Aluminum and Aluminum Alloys." Materials Park, OH: ASM International, 1999.

[10] Erdogan, F., and G.C. Sih. “On The Crack Extension in Plates under Plane Loading and Transverse Shear.” Transactions of ASME. Journal of Basic Engineering, 85-4: 519-527, 1963.

[11] FHWA. “Corrosion Costs and Preventive Strategies in the United States.” 2002.

[12] Gangloff, Richard P. “Environmental Cracking: Corrosion Fatigue.” Corrosion Tests and Standards Manual ASM International, 1–20, 2004.

[13] Genkin, Jean-Marc P. “Corrosion Fatigue Performance of Alloy 6013-T6.” Massachusetts Institute of Technology, 1992.

[14] Gerhardus, H. Koch. “Aircraft, 2.2 Billion per Year.” 2006.

[15] Hawkins, Kari, Redstone, USAG, “Army Attacks Hardware Corrosion.” The Official Homepage of United States Army, 2012.

[16] Hays, R., and G. Keller. “New Technologies and Future Challenges for the Prevention of Corrosion in US DOD Assets.” U.S. Department Of Defense Corrosion Policy and Oversight Office.

[17] Hopper, C.D., and K.J. Miller. “Fatigue Crack Propagation in Biaxial Stress Fields.” The Journal of Strain Analysis for Engineering Design, 12:23–28, 1977.

[18] Joshi S., J. Shewchuk. “Fatigue-Crack Propagation in a Biaxial-Stress Field.” Exp. Mech., 1970.

[19] Kaminski A.A., and N.S. Sailov. “Spreading Of Cracks from the Contours of Elliptical Openings in Brittle Plates under Biaxial Tensile Stresses.” Soviet Applied Mechanics, 11-2: 167-173,1975.

[20] Kopeliovich, Dmitri. “Corrosion Fatigue.” Knowledge Source on Material Engineering.

[21] Lados, D.A., and P.C. Paris. “Parameters and Key Trends Affecting Fatigue Crack Growth: a Tribute to Professor Arthur J. Mcevily’s Contributions.” Materials Science and Engineering: A, 468-470:70-73, 2007.

[22] Lee E.U., and R.E. Taylor. “Fatigue Behavior of Aluminum Alloys under Biaxial Loading.” Engineering Fracture Mechanics, 78:1555–1564, 2011.

[23] Liu A.F., and D.F. Dittmer. “Effect of Multiaxial Loading on Crack Growth.” Volume 2: compilation of experimental data, Northrop Corp Hawthorne, 1978.

[24] McEvily, A.J., and W. Illg. “The Rate of Fatigue Crack Propagation in Two Aluminum Alloys.” NASA TN 4394, 1958.

[25] Megson, T.H.G., Aircraft Structures for Engineering Students, 5th edition, P: 371-372, 2012.

[26] Misak H.E., V.Y. Perel, V. Sabelkin, and S. Mall. “Biaxial Tension-Tension Fatigue Crack Growth Behavior of 2024-T3 under Ambient Air and Saltwater Environments.” Engineering Fracture Mechanics, 118: 83-97, 2014.

[27] Misak H.E., V.Y. Perel, V. Sabelkin, and S. Mall. “Corrosion Fatigue Crack Growth Behavior of 7075-T6 under Biaxial Tension–Tension Cyclic Loading Condition.” Engineering Fracture Mechanics, 106: 38-48, 2013.

[28] Misak H.E., V.Y. Perel, V. Sabelkin, and S. Mall. “Crack Growth Behavior of 7075-T6 under Biaxial Tension–Tension Fatigue.” Int. J Fatigue, 55: 158-165, 2013.

[29] Park, J. K., and A.J. Ardell. “Microstructures of the Commercial 7075 AI Alloy in the T651 and T7 Tempers.” Metall. Trans. A. 14A (1983): 1957. Print.

[30] Parrington, Ronald J. “Fractography of Metals and Plastics.” Practical Failure Analysis, 2002.

[31] Pennisi, Mario S. “Corrosion: Why Apply a Coating.” Coating Fabrication, 1999.

[32] Pocajt, Viktor. “Total Material, Fatigue Properties: Part One.” November 2010.

[33] Norman E. Dowling, “Mechanical Behavior of Materials” , 2013.

[34] Rob, Glossary. “Fatigue (Failure Mechanism).” December 2010.

[35] Roberge, P.R. “Corrosion Engineering: Principles and Practice.” McGraw-Hill, 2008.

[36] Roylance, David. “Introduction to Fracture Mechanics.” Department Of Materials Science and Engineering, Massachusetts Institute of Technology, Cambridge, 2001.

[37] Scheel, E. Jeremy, III. Prevéy, S. Paul, and Douglas J. Hornbach. “The Effect of Surface Enhancement on the Corrosion Properties, Fatigue Strength, and Degradation Of Aircraft Aluminum.” Lambda Research, 2010.

[38] Shanyavskiy, A. “Fatigue Cracking Simulation Based on Crack Closure Effects in Al-Based Sheet Materials Subjected to Biaxial Cyclic Loads.” Engineering Fracture Mechanics, 78:1516- 1528, 2011.

[39] Sih, G.C., “A Special Theory of Crack Propagation.” Mechanics of Fracture, 1: 21-45, 1973.

[40] Sih, G.C., and B.C. Cha. “A Fracture Criterion for Three Dimensional Crack Problems.” Engineering Fracture Mechanics, 6:699-723, 1974.

[41] Sunder, R. “Development Of The Marker-TWIST Load Sequence for Quantitative Fractographic Studies.” International Journal of Fatigue, 2010.

[42] Sunder, R., and B.V. Ilchenko “Fatigue Crack Growth under Flight Spectrum Loading with Superposed Biaxial Loading Due to Fuselage Cabin Pressure.” International Journal of Fatigue, 33:1101–1110, 2011.

[43] Tian, De-Chang, Lu Dau-Quan, and Zhu Jia-Ju. “Crack Propagation under Combined Stresses in Three Dimensional Medium.” Eng.Fract.Mech, 16-1: 5-17, 1982.

[44] Tiroshu, J. “Incipient Fracture Angle, Fracture Loci and Critical Stress for Mixed Mode Loading.” Eng.Fract.Mech, 2-3, 607-616, 1977.

[45] Uhlig, H.H., and R. Winston Revie. “Corrosion and Corrosion Control.” 4th edition, John Wiley and Sons Inc., 2008.

[46] Wikipedia, “Abaqus FEA” https://en.wikipedia.org/wiki/Abaqus. (Accessed June 2016).

[47] Wollmann, M. “Structural Integrity: Stress Corrosion Cracking, Corrosion Fatigue.” Universidad Polytecnica de Madrid, Clausthal University of Technology, May 2012.

[48] Yuuki, R., K. Akita, and N. Kishi. “The Effect of Biaxial Stress and Changes of State on Fatigue Crack Growth Behavior.” Fatigue and Fracture of Engineering Materials and Structures, 12:93-103, 1989.

REPORT DOCUMENTATION PAGE		*Form Approved OMB No. 0704–0188*

1. REPORT DATE (DD–MM–YYYY)	2. REPORT TYPE	3. DATES COVERED *(From — To)*
18/08/2016	Master's Thesis	August 2014 – September 2016

4. TITLE AND SUBTITLE	5a. CONTRACT NUMBER
Effect of Stress Ratio on Fatigue Crack Growth Rate at Notched Hole in 7075-T6 Aluminum Alloy Under Biaxial Fatigue	5b. GRANT NUMBER
	5c. PROGRAM ELEMENT NUMBER
6. AUTHOR(S)	5d. PROJECT NUMBER
Alshahrani Reja, Captain, Royal Saudi Air Force	5e. TASK NUMBER
	5f. WORK UNIT NUMBER
7. PERFORMING ORGANIZATION NAME(S) AND ADDRESS(ES) Air Force Institute of Technology Graduate School of Engineering and Management (AFIT/EN) 2950 Hobson Way WPAFB OH 45433-7765	8. PERFORMING ORGANIZATION REPORT NUMBER AFIT-ENY-MS-16-S-052
9. SPONSORING / MONITORING AGENCY NAME(S) AND ADDRESS(ES) Rich Hays Technical Corrosion Collaboration Office of Secretary of Defense Washington D.C. Tel: (703) 697-3952; E-mail: richard.a.hays18.civ@gmail.com	10. SPONSOR/MONITOR'S ACRONYM(S) TCC OSD
	11. SPONSOR/MONITOR'S REPORT NUMBER(S)

12. DISTRIBUTION / AVAILABILITY STATEMENT
Distribution Statement A: Approved For Public Release; Distribution Unlimited.

13. SUPPLEMENTARY NOTES
This work is declared a work of the U.S. Government and is not subject to copyright protection in the United States.

14. ABSTRACT

This research investigates the behavior of fatigue crack growth rate in both laboratory air and saltwater (3.5% NaCl) environments for notched cruciform specimen made from 7075-T6 aluminum alloy sheet at different stress ratios. With biaxility ratio of 1, and frequency of applied load of 10 Hz, the crack growth behavior was investigated under in-plane biaxial tension-tension fatigue with 0.1, 0.5, 0.7 stress ratios and then compared them to study the effect of stress ratio on the crack growth rate. Finite Element Analysis (FEA) was used to calculate cyclic variation of stress intensity factors (ΔK) at the crack tips. The crack growth rate was observed using optical microscopy. In addition, the test generates more accurate definition of the Walker equation parameters and leads to more accurate prediction of fatigue crack growth rate at different stress ratio. This study shows that there is no effect of the stress ratio on crack path direction. Increase in stress ratio leads to increase in the fatigue crack growth rate under the biaxial loading test. The effective fatigue crack growth rate predicted by Walker equation is very close to the effective fatigue crack growth rate generated by the test in laboratory air and saltwater environments. In the saltwater environment, the corrosion accelerates the crack growth rate.

15. SUBJECT TERMS
Corrosion, Fatigue, Fracture Mechanics, Stress Ratio, Crack Growth Rate, Aluminum Alloy

16. SECURITY CLASSIFICATION OF:			17. LIMITATION OF ABSTRACT	18. NUMBER OF PAGES	19a. NAME OF RESPONSIBLE PERSON
a. REPORT U	b. ABSTRACT U	c. THIS PAGE U	UU	102	Shankar, Mall, Ph. D. (ENY)
					19b. TELEPHONE NUMBER (Include Area Code) (937) (937) 255-6565, ext 4587; Shankar.Mall@afit.edu